SAPIENS DISCOVERIES INTERNACIONAL JOURNAL

SDIJ. 2026;4.2. 008
ISNN: 3091-1788
DOI: https://doi.org/10.71068/SDIJ0108

Article: Original

Rainfall in Honduras between 1998 and 2026: Regional analysis, time series models and projections to 2066

La lluvia en Honduras entre 1998 y 2026: Análisis regional, modelos de series de tiempo y proyecciones a 2066

[1]Marco Antonio Ramos Espinal, [2]Nestor Adrián López Luque.

[1]National Autonomous University of Honduras, Tegucigalpa, Honduras
[2]National Autonomous University of Honduras, Tegucigalpa, Honduras

***Corresponding author:** Marco Antonio Ramos Espinal

Submitted: 08-17-2026 **Revised:** 09-02-2026 **Accepted:** 09-30-2026 **Published:** 10-26-2026

How to cite:

Ramos Espinal, M. A., & López Luque, N. A. (2026). Rainfall in Honduras between 1998 and 2026: Regional analysis, time series models, and projections to 2066. *Sapiens Discoveries International Journal*, *4*(2), 1-36. https://doi.org/10.71068/SDIJ0108

ABSTRACT

Introduction: Precipitation shapes agricultural production, water supply, and hydroelectric generation in Honduras. Differences between its watersheds and the midsummer drought require assessing regional variability, trend stability, and projection uncertainty without confusing statistical changes with confirmed climate signals.
Methods: Monthly series for nine hydrographic regions were analyzed using NASA POWER PRECTOTCORR data for 1998–2025, together with descriptive data for January–August 2026. Regional averages, Theil–Sen slopes, and sensitivity tests for the analysis window and serial correlation were calculated. SARMA and damped Holt–Winters models were compared with climatology over 2019–2025, and exploratory scenarios were developed through 2066. Spatial sampling coverage and approximate calibration of annual prediction intervals were examined.
Results: The area-weighted national precipitation was 1,486 mm annually, compared with 1,572 mm for the unweighted regional average. Regional means ranged from 1,222 to 2,229 mm. All nine slopes were positive and five significant, but none remained significant after excluding 2020–2025. Sampled cells represented 49% of the territory, with duplicate cells in three regions. No model substantially improved upon climatology; approximate coverage of nominal 90% intervals ranged from 41% to 48%. Truncation introduced a 3%–15% bias in the stationary scenario.
Conclusions: These results characterize the NASA POWER product rather than national trends confirmed by rain gauges. Rainfall deficits from May through August 2026 reached 48% on the Pacific slope. Complete spatial averages, cell-level series, and retained validation simulations are required before assigning actual coverage to prediction intervals or using projections in engineering decisions.

Keywords: precipitation; time series; SARMA; Holt-Winters; river basins; dry corridor

RESUMEN

Introducción: La precipitación condiciona la agricultura, el abastecimiento y la hidroelectricidad hondureñas. Sus vertientes y la canícula exigen examinar variabilidad, tendencias e incertidumbre, evitando confundir cambios estadísticos con señales climáticas confirmadas.

©2026 by the Authors. This article is open access and distributed under the terms and conditions under a Creative Commons Attribution 4.0 International License. (CC BY 4.0) https://creativecommons.org/licenses/by/4.0/

Metodología: Se analizaron series de nueve regiones obtenidas de NASA POWER PRECTOTCORR entre 1998 y 2025, y datos de enero a agosto de 2026. Se calcularon medias, pendientes Theil-Sen y pruebas de sensibilidad. Los modelos SARMA y Holt-Winters amortiguado se contrastaron con la climatología durante 2019-2025 y se proyectaron escenarios hasta 2066. Se evaluaron cobertura espacial y calibración aproximada de intervalos.
Resultados: La precipitación nacional ponderada por superficie fue de 1 486 mm anuales, frente a 1 572 mm como promedio simple. Los promedios regionales variaron entre 1 222 y 2 229 mm. Las nueve pendientes fueron positivas, cinco significativas, pero ninguna mantuvo significación al excluir 2020-2025. El muestreo cubrió 49 % del territorio, con celdas duplicadas en tres regiones. Los modelos apenas mejoraron la climatología; la cobertura aproximada de intervalos nominales del 90 % osciló entre 41 % y 48 %. El truncamiento produjo sesgos del 3 % al 15 % en el escenario estacionario.
Conclusiones: Los resultados describen propiedades del producto NASA POWER, no tendencias nacionales confirmadas mediante estaciones. La sequía de mayo a agosto de 2026 alcanzó déficits de hasta 48 % en la vertiente pacífica. Se requieren promedios espaciales completos, series por celda y simulaciones de validación conservadas antes de validar intervalos y aplicar proyecciones a la ingeniería.

Palabras clave: precipitación; series de tiempo; SARMA; Holt-Winters; cuencas hidrográficas; corredor seco

INTRODUCTION

Honduras maintains a relationship between rainfall patterns, agricultural production, and water security. Of the national water withdrawals, 52.40% is used for irrigation, 14.32% for human consumption, and 13.63% for hydroelectric generation (1). In 2024, hydroelectric plants contributed 30.88% of the 12,416.80 gigawatt hours generated, while thermal generation with bunker and diesel accounted for 40.50% (2). In particular, the two basic grain cycles are exposed to changes in the onset of rainfall and in the heat wave.

The effects of hydrometeorological variability have been severe. Hurricane Mitch, between October and November 1998, caused 5,657 deaths and 8,058 disappearances, in addition to damages estimated at 3,800 million dollars and substantial damage to crops (3). More than two decades later, tropical storm Eta and Hurricane Iota caused effects of 52,099 million lempiras in 2020, of which 35,509 million corresponded to the productive sector (4). At the opposite extreme, the 2015 drought caused losses of more than 80% in certain basic crops and particularly affected subsistence farmers (5).

Honduran climate planning instruments recognize these differences, although their horizons and methods are not equivalent. The First Adaptation Communication contemplates, under RCP 8.5 by 2080, annual precipitation reductions of up to 10% and greater decreases in the June-August quarter for certain areas (5). The National Plan for Drinking Water and Sanitation incorporates scenarios of lower water availability and adaptation needs in supply systems (6). These physical projections should not be confused with statistical extrapolations from a historical series.

The problem of spatial scale has acquired special importance in Central America. González-Méndez et al. compared grid precipitation products with meteorological stations in the region and documented relevant differences in biases, correlation, and trend representation, even in Honduras (7). Their study shows that the nominal resolution of a product does not guarantee that local variations are adequately represented. Therefore, a territorial average requires distinguishing the

extent of the regions from the area effectively covered by the cells consulted. A weighting of regions by their areas does not replace the spatial integration of the cells that make up each region.

The nature of the extremes poses a second analytical requirement. Alfaro-Córdoba et al. studied CLIMDEX indices in Central America and observed that the signals of change in extreme rainfall are spatially heterogeneous, although some intense episodes show identifiable trends (8). A year can bring together extraordinary storms and, simultaneously, deficits during critical months for planting. Nor is it correct to interpret the slope of a few decades as if it were equivalent to a long-term climate projection. It is necessary to examine the sensitivity of trends to autocorrelation, temporal selection, and recent wet episodes.

Prediction adds different difficulties from those of historical description. Kowal et al. compared dynamic, statistical, and hybrid seasonal forecasts for Central America, finding capacities that vary by area and by rainy season (9). Andrade-Gómez and Cavazos, in evaluating historical meteorological droughts and regional simulations, also highlighted the geographic heterogeneity of water deficit (10). For a national analysis, this implies first establishing a climatological reference and then verifying whether more complex models offer measurable out-of-sample improvements. Predictive intervals should be evaluated with the same procedure that generates them and not only through approximate historical distributions.

Central American seasonality also requires considering the mechanisms that cause the heat wave. García-Franco et al. examined the subseasonal prediction of the Mesoamerican rainy season and pointed out differences in the representation of the mid-summer dry period (11). Peña Salinas documented links between forest management practices and environmental conditions relevant to territorial resilience in a Honduran micro-basin (12). Rodríguez Saldaña and Rodriguez Estrella addressed the health risks associated with climatic extremes and the needs for prevention (13). These contributions offer complementary contexts, but do not replace the regional measurement of rainfall; therefore, they are considered antecedents on exposure and adaptation, not validations of the reanalysis used in this research.

From the productive perspective, Merino Olivo examined the relationship between climate variability and food resilience in Ecuadorian peasant communities, with attention to adaptation decisions in the face of droughts and intense rainfall (14). In Honduras, a gap persists between the general climate change scenarios and the comparable monthly series of its different hydrographic regions. Consequently, this work characterizes precipitation from 1998 to 2025 using NASA POWER, examines the first eight months of 2026, contrasts the robustness of trends, and validates SARMA and Holt-Winters models. In addition, it presents exploratory scenarios up to 2066, explicitly differentiating them from calibrated forecasts and CMIP6 physical scenarios, with explicit limits for a responsible scientific interpretation of each outcome.

METHOD

2.1 Study area and regionalization

Honduras is located between 13 and 16 degrees north latitude. Its rainfall regime is governed by seasonal migration from the intertropical convergence zone, the northeasterly trade winds, and the Atlantic hurricane season. The territory is organized into 21 main hydrographic basins, 14 of which drain into the Caribbean Sea and 5 into the Pacific Ocean; the three largest are those of the Patuca River, with 23,898 square kilometers, Ulúa, with 22,817, and Aguán, with 10,266 (1).

For the analysis, nine regions were defined from these basins. Each department was assigned in its entirety to the region that contains most of its territory, which produces real administrative boundaries and not watersheds. The simplification makes it possible to link the results with the country's sectoral statistics, which are published by department, at the cost of an approximate allocation in the departments crossed by more than one basin, such as Comayagua and Yoro. The cartographic boundaries come from the Natural Earth set of first-level administrative units (15) (Figure 1). On these same polygons, in a cylindrical projection of equal areas, the area of each region was calculated: the nine add up to 112,236 square kilometers and range from 257 in the Bay Islands to 31,519 in the Patuca basin (Table S1).

Figure 1.

Hydrographic regionalization used and location of sampling points

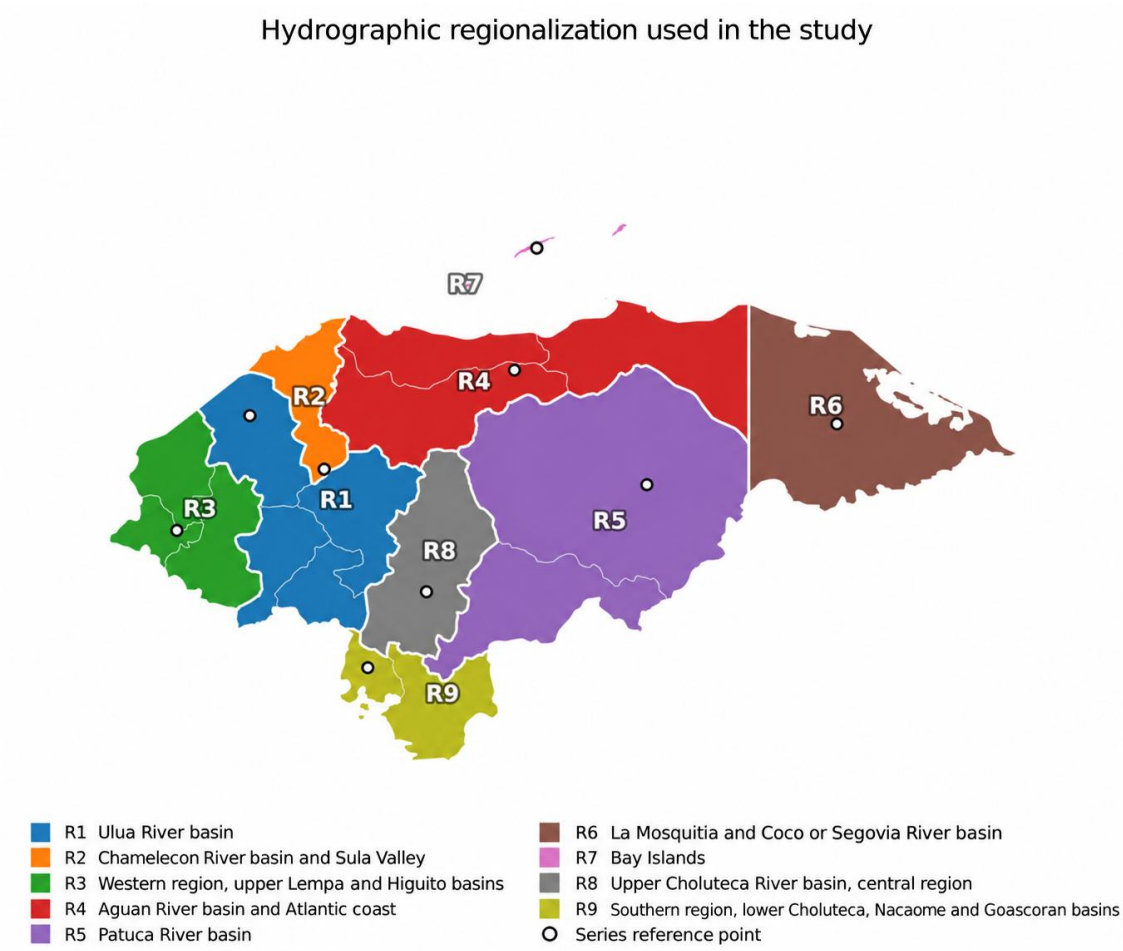

https://doi.org/10.71068/SDIJ0108

Note: Prepared by the author with administrative boundaries of Natural Earth. The boundaries are departmental, grouped by dominant basin.

2.2 Precipitation Data

Precipitation comes from the PRECTOTCORR parameter of the NASA POWER system, version 2.9.8 (16), which redistributes the output of the MERRA-2 reanalysis of NASA's Center for Global Modeling and Assimilation (17). The suffix CORR indicates that the precipitation of the model was corrected against surface observations. The data is provided as a daily average sheet in millimeters per day for each month and converted to a monthly sheet by multiplying by the actual number of days in the month, with the leap years considered.

The modeling period covers January 1998 to December 2025, i.e. 336 monthly observations per region, and the models used in the projections were readjusted with that complete series after validation. The first eight months of 2026 were reconstructed from the daily interface of the same system, averaging the values of each month, and are used only to describe the current season. Within each region, three points were selected by grouping by k-means on a regular mesh of points inside the regional polygon, and the regional series was obtained as a simple average of the series that NASA POWER returns for those points.

The representativeness of this sampling was evaluated quantitatively. Each query returns the value of the MERRA-2 cell containing the point, 0.5 degrees latitude by 0.625 degrees longitude, about 3 700 square kilometers, and the surface area of these cells varies less than 2 percent between 13 and 16.5 degrees latitude, so that the simple average of different cells is effectively equivalent to an area-weighted average. Assigning the 27 points to the mesh, however, found that in three regions, R2, R3, and R8, two points fall in the same cell; NASA POWER warns that queries below their resolution may return the same data (16).

In these regions, the repeated cell weighs two-thirds of the average. If the weights were assigned according to the area of the region that falls within each sampled cell, the repeated cell would weigh 0.69 in R2, 0.60 in R3, and 0.50 in R8, so that the doubling approximates an area weighting in the first two and overweights one cell in the third. The sampled cells cover between 32 percent of the regional area, in the Patuca basin, and 92 percent, in the Bay Islands, whose cells are mostly sea, and together 49 percent of the national territory (Table S1).

The national average was calculated in two ways. The simple average of the nine regions treats the Bay Islands and the Patuca basin equally, whose area is about 120 times larger, so that it does not represent the territorial average rainfall. That is why an area-weighted average of each region was also calculated. Both are reported, and the national average refers to the weighted average hereafter unless otherwise indicated.

The spatial coverage assessment allowed for recognition of how much of each region was represented by the queries, but did not provide series for all the cells in the region. The averages and trends in the tables retain the original estimate of three points per region, including cell repetition in R2, R3, and R8. In R8, in particular, the implicit weighting of the duplicate cell (two-thirds) exceeds the estimated

surface share (approximately one-half). Thus, the national weighted average remains a synthesis of sampled regional averages, not a full average per pixel. The final correction requires the monthly series per cell and the spatial intersection of each with the regional polygon; the aggregate data of the supplementary material do not allow for the recalculation of their slopes or projection scenarios without introducing additional assumptions.

The choice of a reanalysis product responds to a restriction of availability: Honduras does not publish continuous monthly rainfall series per season for the entire period in an open format, and working with field records would force filling gaps and homogenizing networks that changed in composition over three decades.

2.3 Exploratory analysis and statistical testing

For each region, the mean, standard deviation, and coefficient of variation of the annual totals were calculated, and the average month-to-month annual cycle. Stationarity was examined with the augmented Dickey-Fuller test, whose null hypothesis is the presence of a unit root, and with the KPSS test, which takes stationarity as the null hypothesis. The trend was assessed with the nonparametric Mann-Kendall test (18,19) and its magnitude was estimated with the Theil-Sen slope, defined as the median of all slopes between pairs of observations (20), an estimator that resists well the outliers introduced by years such as 1998, 2020, and 2022.

The Mann-Kendall test assumes independent observations, and the positive autocorrelation inflates its false positive rate. Therefore, two versions were applied to correct it: that of Hamed and Rao, which adjusts the variance of the statistic according to the autocorrelation of the ranges (21), and the pre-bleaching without trend of Yue et al. (22). The stability of the slopes was also examined by repeating the calculation in three alternative windows: from 1998 to 2019, which excludes the final wet block; from 1998 to 2022, and from 2001 to 2025, which excludes the first years of the record. These tests were calculated on the annual totals of Table S5, rounded to the millimeter.

2.4 Time series models

The first model family is the SARA class, which combines an autoregressive part and a moving average part in the monthly frequency with their equivalents in the twelve-month seasonal frequency. A SARMA(p, 0, q)(P, 0, Q) model of period 12 is written as

$$\Phi(B^{12})\,\varphi(B)\,(y_t - \mu) = \Theta(B^{12})\,\vartheta(B)\,\varepsilon_t$$

where B is the lag operator, ϕ and θ are the ordinary polynomials of order p and q, Φ and Θ are the seasonal polynomials of order P and Q, μ the mean of the series and ε a white noise of constant variance. The orders were chosen by exhaustive search on a grid with p, q, P and Q between 0 and 2, selecting the model with the lowest criterion of Akaike information corrected for finite samples, with estimation by maximum likelihood in representation of state space.

The second family is exponential smoothing with level, trend, and seasonality components in its damped trend additive formulation (23), whose update equations are

$$l_t = \alpha\,(y_t - s_{t-12}) + (1-\alpha)\,(l_{t-1} + \varphi\, b_{t-1})$$

$$b_t = \beta\,(l_t - l_{t-1}) + (1-\beta)\,\varphi\, b_{t-1}$$

$$s_t = \gamma\,(y_t - l_{t-1} - \varphi\, b_{t-1}) + (1-\gamma)\, s_{t-12}$$

with l the level, b the trend, s the seasonal factor and α, β, γ the smoothing parameters. The parameter ϕ dampens the trend: with ϕ less than one, the projected slope is turned off geometrically instead of extending in a straight line. The additive variant was used because the southern region has months with precipitation close to zero and the multiplicative variant requires strictly positive values.

2.5 Restriction to stationary class

The standard practice in monthly seasonal series is to differentiate once at the ordinary frequency and once at the seasonal frequency. This approach works over month horizons, but an integrated model describes a process whose forecast variance grows without limit with the horizon. By projecting 492 months, the preliminary versions of this analysis produced intervals ranging from 0 to 19,000 millimeters per year in some regions, a range that does not describe uncertainty but the absence of information. The annual precipitation of a place is bounded by physics: it cannot be negative or grow indefinitely, and a model whose variance diverges contradicts that property. For this reason, the models used to project were restricted to the stationary class, with d and D equal to zero, where the forecast mean converges to the long-run mean and the variance to the unconditional variance. The integrated models were retained only as a comparison term in validation, where the horizon is short.

2.6 Projection scenarios

Instead of presenting a single model as a forecast, three scenarios were projected that respond to different assumptions about the continuity of the observed trend. The E1 scenario, stationary, uses the SARMA model without a trend component and assumes that the recent rise is a low-frequency fluctuation that will end up reversing; it is the reference scenario. The E2 scenario, with a damped trend, uses the Holt-Winters model and assumes that the trend continues but is extinguished. The E3 scenario, with a sustained trend, incorporates a deterministic linear trend as an external regressor of the SARMA model and assumes that the slope from 1998 to 2025 remains unattenuated for forty more years. E2 and E3 are treated as exploratory scenarios: they describe the consequences of an assumption on the trend and have no demonstrated predictive capacity.

2.7 Validation and prediction intervals

The models were adjusted over 252 months, from January 1998 to December 2018, and the 84 months from 2019 to 2025 were forecast without reusing these data. Performance was measured with the root mean square error, the mean absolute error and the percentage mean absolute error, calculated on the monthly values and on the annual totals. As a reference, climatology was included, which forecasts for each future month the historical average of that month in the adjustment period, and the SARIMA(0,1,1)(0,1,1) model of period 12, a classic integrated specification for seasonal monthly series.

The intervals were estimated by simulation and not by the analytical formula of variance. From each fitted model, 5,000 monthly trajectories of 492 steps were generated, the negative values that the additive model can produce were truncated by zero, and the twelve months of each year were added together to obtain 5,000 annual totals per projected year. The 5th and 95th percentiles of this distribution delimit the 90 percent prediction interval, and the 2.5 and 97.5 percentiles delineate the 95 percent prediction interval. These are prediction intervals for the annual total for a given year, not prediction intervals for a parameter. The simulation propagates the variability of model innovations and the correlation between the twelve months of the same year, but does not incorporate the uncertainty of the estimated parameters, the uncertainty of the model selection, the uncertainty of the reanalysis product, or the uncertainty of future climate forcing, so the intervals should be read as a lower bound of the total uncertainty.

An approximation to the coverage of annual intervals was explored with the 63 totals observed between 2019 and 2025, distributed in nine regions and seven years (24); it does not correspond to a check of the intervals actually generated by each model during validation. As the simulated trajectories of the validation were not preserved, the coverage was calculated with the stationary distribution of the annual totals adjusted for 1998-2018, in its normal, gamma and empirical versions. This distribution is an adequate approximation to that of E1: in 2030 the amplitude of the 90 percent interval of E1 is equivalent to between 0.84 and 1.02 times that of a normal distribution with the observed standard deviation.

Truncation at zero introduces a positive bias, because it eliminates the negative tail of the monthly distribution without compensating for it. To quantify it, the mean level of the E1 medians between 2027 and 2066 was compared with the observed mean from 1998 to 2025: in a stationary model without a trend, this difference does not have a climatic origin. The correction consisted of multiplying the medians and percentiles of E1 of each region by the quotient between the two quantities, an operation that preserves the non-negativity. As a contrast, a gamma distribution was adjusted for maximum likelihood to the annual totals from 1998 to 2025, a stationary specification that only admits positive values, and its quantiles were compared with those of corrected E1.

The analysis was performed in Python 3.11 with the statsmodels 0.15, pandas, numpy, scipy, scikit-learn, geopandas, pymannkendall, and matplotlib libraries.

RESULTS

3.1 Magnitude and regional distribution of rainfall

The average annual rainfall from 1998 to 2025 was 1,486 millimeters weighted by area and 1,572 millimeters as a simple average of the nine regions. The difference of 86 millimeters is due to the fact that the Patuca basin, one of the driest, occupies 28 percent of the territory, while the Bay Islands, the rainiest, weigh 0.2 percent. Between the regional extremes there are 1,007 millimeters, a factor of 1.8: the Bay Islands receive 2,229 millimeters per year and La Mosquitia 2,012, while the upper basin of the Choluteca River, where Tegucigalpa is located, remains at 1,222 and the Patuca at 1,233 (Table 1).

The coefficient of variation ranges from 20.2 per cent in La Mosquitia to 31.4 per cent in the western region. The wettest regions are also the most stable, and those in transition between slopes are the most erratic. The annual minimums of the record reach values typical of semi-arid zones: the upper Choluteca basin fell to 661 millimeters in 2001, when the western region registered 901 millimeters and the Patuca 750.

Table 1.

Hydrographic and statistical regions of annual precipitation, 1998 to 2025

Region	Departments	Slope	Medium (mm)	OD (mm)	CV (%)	Minimum (mm)	Maximum (mm)
R1 Ulúa	Comayagua, Santa Barbara, La Paz, Intibucá	Caribbean	1 361	388	28,5	838	2 451
R2 Chamelecón	Cortés	Caribbean	1 592	409	25,7	944	2 676
R3 West	Copán, Ocotepeque, Lempira	Both	1 428	449	31,4	901	2 788
R4 Aguán	Atlántida, Colón, Yoro	Caribbean	1 706	430	25,2	1 089	2 597
R5 Patuca	Olancho, El Paraíso	Caribbean	1 233	307	24,9	750	2 041
R6 Mosquitia	Thank goodness	Caribbean	2 012	406	20,2	1 383	2 948
R7 Bay Islands	Bay Islands	Caribbean	2 229	465	20,9	1 255	3 049
R8 Choluteca Alta	Francisco Morazán	Pacific	1 222	331	27,1	661	2 065
R9 On	Choluteca, Valle	Pacific	1 361	335	24,6	793	2 032
National, Simple Average	Simple average of the nine regions		1 572	391	25,4	1 080	2 323
National, weighted	Area-weighted		1 486	374	25,5	1 027	2 164

Note: SD is the standard deviation and CV is the coefficient of variation. In the national rows, SD and CV are the simple or weighted average of the regional values, and the minimum and maximum correspond to the respective national series in 2019 and 2022. Prepared by the authors with data from NASA POWER (16).

3.2 Annual cycle and heat wave

The average annual cycle confirms the existence of two well-differentiated regimes (Figure 2; Table S8). On the Pacific slope, the season starts in May with a sharp jump: the southern region goes from 37 millimeters in April to 190 in May, and the upper Choluteca basin from 40 to 140. June marks the first peak. July brings the fall of the heat wave, which takes the southern region from 229 millimeters

in June to 128 in July. September and October bring the second peak, higher than the first in the south, with 271 and 237 millimeters. Measured as the fall in July compared to June, the heat wave reaches 44 percent in the southern region, 32 percent in the upper Choluteca basin, 29 percent in the Ulúa basin, and 26 percent in the west.

On the Caribbean coast, the pattern is unimodal and displaced. The Bay Islands receive 186 millimeters in January, when the southern region barely registers 6; its maximum comes in October, with 337 millimeters, and November and December continue to be rainy months, with 330 and 221. The heat wave is diluted or disappears: in La Mosquitia, July is one of the rainiest months, with 265 millimeters.

Figure 2.

Average annual precipitation cycle by region, 1998 to 2025

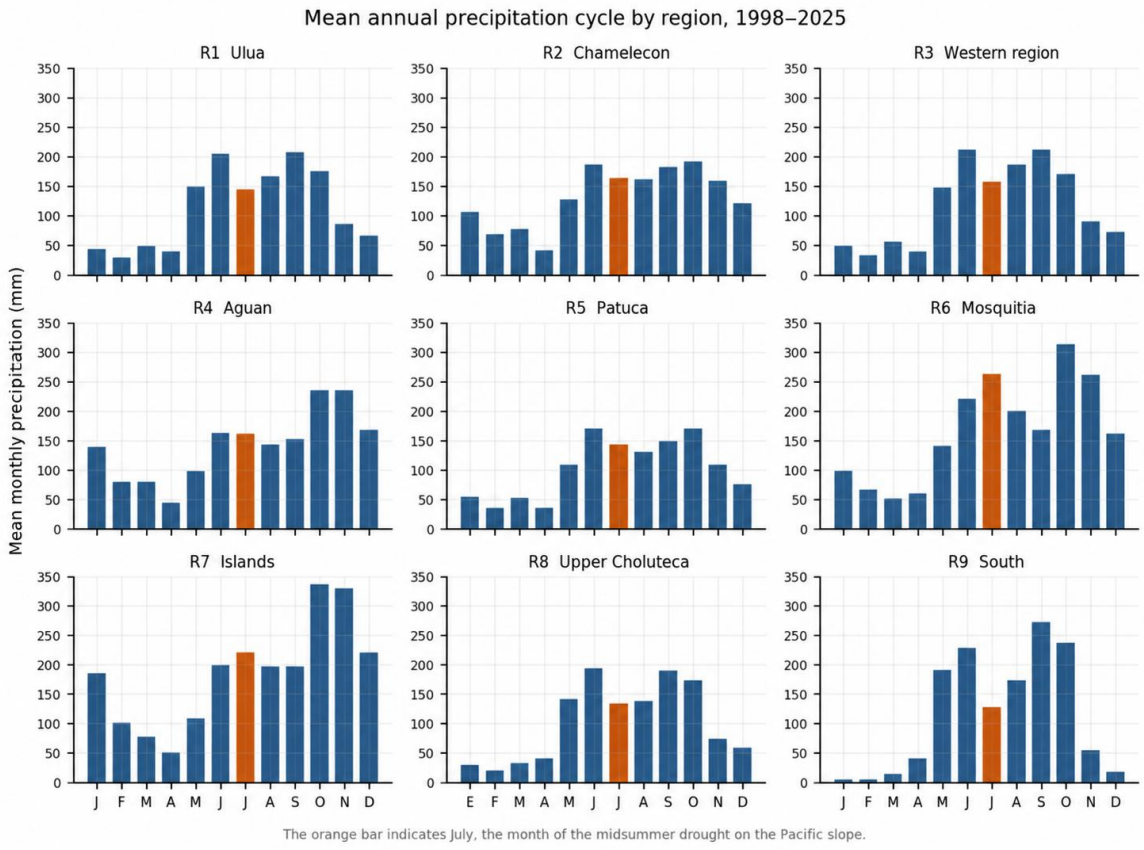

Note: Prepared by the authors with data from NASA POWER (16). The orange bar indicates July, the month of the heat wave on the Pacific slope.

3.3 Year-on-year variability and trends

The national average ranged from 1,027 millimeters in 2019 to 2,164 in 2022. The five driest years were 2019, 2001, 2006, 2002 and 2004, and the five wettest were 2022, 2020, 2025, 2024 and 2017. This ordering coincides with documented events: 2001 and 2019 were years of severe drought in the dry corridor and 2020 the year of Eta and Iota.

https://doi.org/10.71068/SDIJ0108

Mitch's year deserves a methodological comment. On the annual scale, 1998 appears with a negative anomaly of 5 percent, because Mitch was a five-day event and not a one-year event. On the monthly scale, its footprint is unequivocal: October 1998 recorded 368 millimeters in the Ulúa basin compared to an average of 175 for that month, and 731 millimeters in the Bay Islands compared to 337. The annual totals describe water availability, not disaster risk, which depends on intensity on hourly and daily scales.

The correlations between regions draw three blocks. The first groups the Ulúa, the Chamelecón and the west, with coefficients of 0.84 to 0.97. The second brings together the Aguán, the Patuca and the Bay Islands, with values of 0.88 to 0.93. The third is formed by the upper Choluteca basin and the southern region, correlated at 0.86. La Mosquitia behaves as an exception: its highest correlation with any other region is 0.62, which suggests a different forcing.

The nine regions show positive Theil-Sen slopes, ranging from 13.7 millimeters per year in the southern region to 37.5 millimeters in the Aguán region (Table 2). The Mann-Kendall test declares these significant trends at 5 percent in the west, the Aguán, the Patuca, the Bay Islands, and the upper Choluteca basin. In the Ulúa and La Mosquitia regions, the p-value is just above the threshold, at 0.0505 and 0.0553. The national average increases by 25.6 millimeters per year, with a p-value of 0.001. The stationarity tests leave an ambiguous picture: ADF rejects the unit root in all nine regions and KPSS rejects stationarity in five, which in practice describes stationary series around a trend (Table S9).

Table 2.

Annual precipitation trend by region and its robustness to autocorrelation and the analysis window, 1998 to 2025

Region	Theil-Sen 1998-2025 (mm/year)	MK p	MK Hamed -Rao p	TFPW p	Theil-Sen 1998-2019	p 1998-2019	Theil-Sen 2001-2025	p 2001-2025
R1 Ulúa	+16,3	0,051	0,048	0,123	+1,9	0,933	+25,5	0,009
R2 Chamelecón	+15,9	0,199	0,199	0,211	−0,2	1,000	+28,4	0,042
R3 West	+17,3	0,023	0,002	0,073	+5,1	0,516	+26,1	0,014
R4 Aguán	+37,5	0,000	0,000	0,000	+19,3	0,055	+47,4	0,000
R5 Patuca	+20,9	0,002	0,002	0,001	+12,3	0,195	+28,9	0,001
R6 Mosquitia	+19,7	0,055	0,055	0,022	+10,4	0,398	+23,6	0,042
R7 Bay Islands	+25,1	0,023	0,023	0,037	+11,8	0,463	+35,2	0,010

Region	Theil-Sen 1998-2025 (mm/year)	MK p	MK Hamed -Rao p	TFPW p	Theil-Sen 1998-2019	p 1998-2019	Theil-Sen 2001-2025	p 2001-2025
R8 Choluteca Alta	+20,3	0,015	0,001	0,008	+1,8	0,866	+27,9	0,003
R9 On	+13,7	0,105	0,105	0,055	+3,5	0,756	+22,9	0,025
National	+25,6	0,001	0,001	0,001	+10,5	0,236	+31,9	0,000

Note: MK is the Mann-Kendall test; Hamed-Rao and TFPW (pre-bleaching without trend) are versions that correct for autocorrelation. Columns 2 and 3 of the regional rows were calculated on the basis of the unrounded data; the others on the rounded annual totals of Table S5, which brings the Mann-Kendall p-value of the Ulúa from 0.051 to 0.048. The national row corresponds to the area-weighted average. Prepared by the authors with data from NASA POWER (16).

Figure 3.

Observed annual precipitation and Theil-Sen trend by region, 1998 to 2025

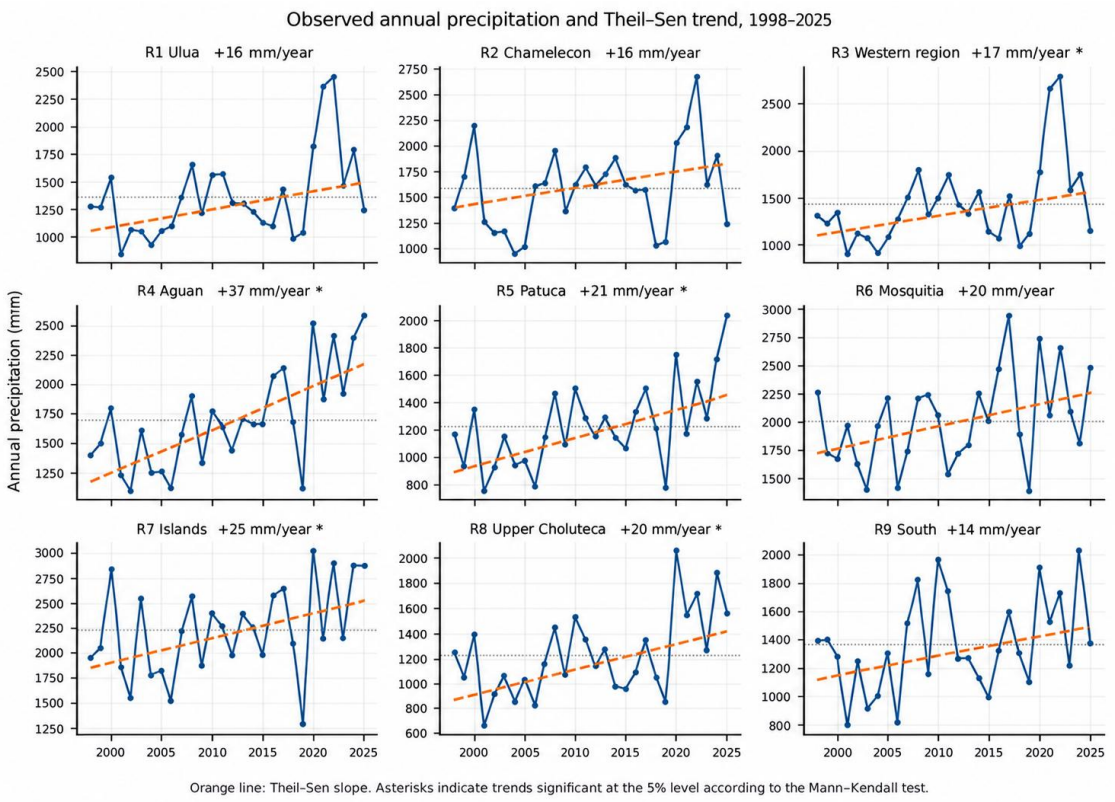

Note: Prepared by the author with data from NASA POWER (16). The asterisk marks significant trends at 5 percent according to Mann-Kendall.

Figure 3 makes it necessary to qualify these slopes, and the robustness tests confirm caution (Table 2). The first-order autocorrelation of the annual totals ranges from −0.11 to 0.56 and is higher in the west and the Ulúa. Corrected by the Hamed and Rao method, the significance is maintained in the same five regions, and the Ulúa remains at the threshold; with the pre-bleaching without a trend, it

is maintained in the Aguán, the Patuca, the Bay Islands and the upper Choluteca basin, it is lost in the west (p = 0.073) and appears in La Mosquitia (p = 0.022). The dependence on the window is much stronger.

The period from 2020 to 2025 includes four of the five wettest years of the three decades; when excluded, the slopes from 1998 to 2019 fall to values of −0.2 to 19.3 millimeters per year and none are significant at 5 percent, with the Aguán at the limit (p = 0.055). With the window from 1998 to 2022 only the west, the Aguán and the Patuca retain significance, and when excluding the first three years, which include the dry 2001, all nine regions become significant. The positive trend exists in the NASA POWER series, but its magnitude and significance depend on a final six-year wet block.

3.4 The 2026 season

The first eight months of 2026 contradict the trend of previous years and coincide with an ongoing supply crisis. The accumulated from January to August is misleading: in the upper Choluteca basin it was 29 percent above normal, a surplus that is almost entirely due to an anomalous April with 319 millimeters compared to an average of 40.

When looking at the rainy season, from May to August, the picture is reversed (Figure 4). The southern region accumulated 373 millimeters against an average of 717, that is, 48 percent less. The Ulúa basin was 37 percent lower, the west 36 percent and the upper Choluteca basin 35 percent. July was the hardest hit month on the Pacific and western slopes, with deficits of between 40 and 71 percent in five of the nine regions. The Caribbean coast and La Mosquitia, on the other hand, had a normal or slightly wet season.

Figure 4.

Precipitation anomaly from May to August 2026 compared to the average 1998 to 2025

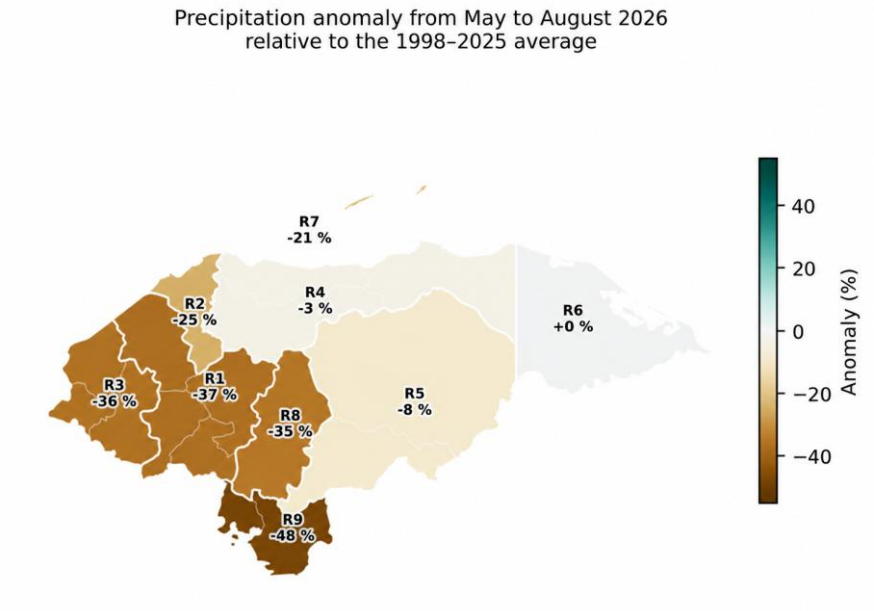

https://doi.org/10.71068/SDIJ0108

Note: Prepared by the authors with data from NASA POWER (16). The deficit is concentrated on the Pacific slope and in the west.

3.5 Model performance

The search by information criterion selected parsimonious specifications. The dominant seasonal structure combines a seasonal autoregressive of order one with a seasonal moving average of order one, present in seven of the nine regions, and in the ordinary part an autoregressive of order two predominates. The Ljung-Box test on 24 lags does not reject the absence of autocorrelation in eight of the nine regions; the exception is the West, with a p-value of 0.029, which is also the region with the highest coefficient of variation. In the Holt-Winters fit, parameters β and γ were estimated at zero in the nine regions and the α-level parameter was between 0.014 and 0.159, so that the model is mainly based on the historical mean.

The out-of-sample validation yields the most informative result of the work (Table 3). The average absolute percentage error over annual totals is 24.7 percent for the best model, 26.3 percent for the stationary model, and 26.7 percent for climatology. The difference between fitting a time-series model and repeating the historical average for each month is less than two percentage points.

Table 3.

Model performance in out-of-sample validation, 2019 to 2025

Model	Annual RMSE (mm)	Annual MAE (mm)	Annual ASM (%)	Monthly RMSE (mm)
E3 SARMA trending	530	445	24,7	102,6
E1 stationary SARMA	612	512	26,3	105,6
Climatology (reference)	616	517	26,7	105,7
E2 Holt-Winters amortized	644	537	27,9	107,8
SARIMA(0,1,1)(0, $1,1)_{12}$ integrated	658	561	30,0	109,0

Note: Values averaged over the nine regions. RMSE is the root of the mean square error, MAE the mean absolute error, and MAPE the percentage mean absolute error. Authors' elaboration.

The order of the models also informs. The only one that clearly exceeds climatology is the one that incorporates a linear trend, and it does so because the validation window falls in the wet section of the record. This success indicates that the trend continued during the seven years of the test, a much weaker statement than that it will continue. The integrated model came in last place: by differentiating, it anchors the forecast in the last observations and drags its noise forward.

The approximate coverage calculated with stationary historical distributions was much lower than the nominal one; it should not be confused with the coverage of the intervals simulated by the models evaluated. Of the 63 annual totals observed between 2019 and 2025, the 90 percent interval of the

stationary distribution contained 30 in the normal version (48 percent), 28 in the gamma (44 percent), and 26 in the empirical (41 percent); for the 95 percent range the coverages were 59, 67 and 52 percent. The failure is asymmetric: with the gamma distribution, 31 of the 35 values outside the 90 percent range were above the upper limit and only 4, 6 percent of the total, below the lower limit, close to the nominal 5 percent. The approximate distributions underestimated wet years such as 2020-2022; This result warns of a possible lack of calibration, but the models' own coverage can only be established by preserving their validation simulations.

3.6 Projections to 2066

Without correction, the stationary scenario brings the rainfall of 2066 to 1 701 millimeters as a simple average of the regions and to 1 619 with weighting by area. This increase does not come from a trend incorporated into the model, which does not have one, but from the truncation at zero: in the dry months of the Pacific regions the model produces negative values without physical sense that are brought to zero, and this operation raises the annual total. The average level of E1 between 2027 and 2066 exceeds the average observed by between 56 millimeters in the Chamelecón (3.5 percent) and 201 in the Aguán (11.8 percent), with a relative maximum of 15.0 percent in the upper Choluteca basin; in the national average the excess is 152 millimeters (Table S10). It is a numerical artifact and not a physical signal, so all the E1 figures that follow are corrected.

Corrected, E1 reproduces the climatology of the adjustment period with a flat trajectory: the national median is 1 468 millimeters in 2066, compared to 1 486 observed, and the geography of rainfall is preserved, with La Mosquitia and the Bay Islands as the wettest regions and the Patuca and the upper Choluteca basin as the driest (Table 4). The amplitude of its intervals increases little along the horizon, a property that was sought when restricting the models to the stationary class. The gamma distribution, which respects non-negativity by construction, produces medians that differ less than 3 percent from those of E1 corrected; its 90 percent intervals are narrower in the Ulúa and the west, where those of E1 widen with the horizon, and similar in the rest (Table S10).

Table 4.

Projected annual precipitation for 2066 according to scenario, in millimeters

Region	Observed 1998-2025	E1 corrected medium	E1 IP 90 %	E1 IP 95 %	E2 median	E3 median
R1 Ulúa	1 361	1 365	646 a 2 117	543 a 2 275	1 396	2 354
R2 Chamelecón	1 592	1 584	886 a 2 341	751 a 2 513	1 338	2 356
R3 West	1 428	1 410	586 a 2 406	443 a 2 614	1 346	2 498
R4 Aguán	1 706	1 671	1 052 a 2 310	929 a 2 449	2 452	3 713
R5 Patuca	1 233	1 204	770 a 1 694	683 a 1 790	1 736	2 437
R6 Mosquitia	2 012	2 006	1 368 a 2 680	1 248 a 2 820	2 219	3 097

https://doi.org/10.71068/SDIJ0108

Region	Observed 1998-2025	E1 corrected medium	E1 IP 90 %	E1 IP 95 %	E2 median	E3 median
R7 Bay Islands	2 229	2 223	1 521 a 2 959	1 393 a 3 089	2 578	3 456
R8 Choluteca Alta	1 222	1 200	763 a 1 680	683 a 1 771	1 632	2 400
R9 On	1 361	1 366	926 a 1 832	849 a 1 931	1 646	2 188
National, Simple Average	1 572	1 559			1 816	2 722
National, weighted	1 486	1 468			1 831	2 742

Note: E1 is the stationary scenario corrected for truncation bias (Table S10); E2, with a damped trend, and E3, with a sustained trend, are exploratory scenarios. The values are medians of 5 000 simulated trajectories for 2066 and the intervals are predictive for the annual total for that year. The national rows combine the regional medians as a simple average or area-weighted. Prepared by the authors with data from NASA POWER (16).

The damped trend scenario puts the national average at 1 831 millimetres, but its intervals are its weak point. The average amplitude of the 95 per cent interval goes from 1 333 millimetres in 2026 to 2 880 in 2040 and 4 141 in 2066; in three regions the lower limit reaches zero before 2066 and the upper limit exceeds 6 000 millimetres. The cause is structural: exponential smoothing with additive errors assumes a level that follows a random walk, so that the forecast variance grows linearly with the horizon even though the trend is damped. The damping controls the mean and not the variance, and the scenario is no longer interpretable from about 2040. For this reason, E2 is presented only as an exploratory scenario and is not used as a limit of any planning range.

The sustained trend scenario yields 2 742 millimeters nationally (2 722 as a simple average), 84 percent above the observed average, with the Aguán basin going from 1 706 to 3 713 millimeters. These values would make the Aguán valley one of the rainiest areas in Central America and should not be read as a forecast. It should be noted that the deterministic trend is significant at 5 percent in only three regions: the Aguán, with 36.6 millimeters per year and a p-value of 0.001, the Patuca with 22.1 and a p-value of 0.011, and the upper Choluteca basin with 21.4 and a p-value of 0.019. Figure 5 brings together the observations, the corrected E1 trajectory with its prediction intervals, and the E2 and E3 values in 2066.

Figure 5.

Observations from 1998 to 2025 and projections to 2066 by region, with 90 and 95 percent prediction intervals of the corrected stationary scenario

https://doi.org/10.71068/SDIJ0108

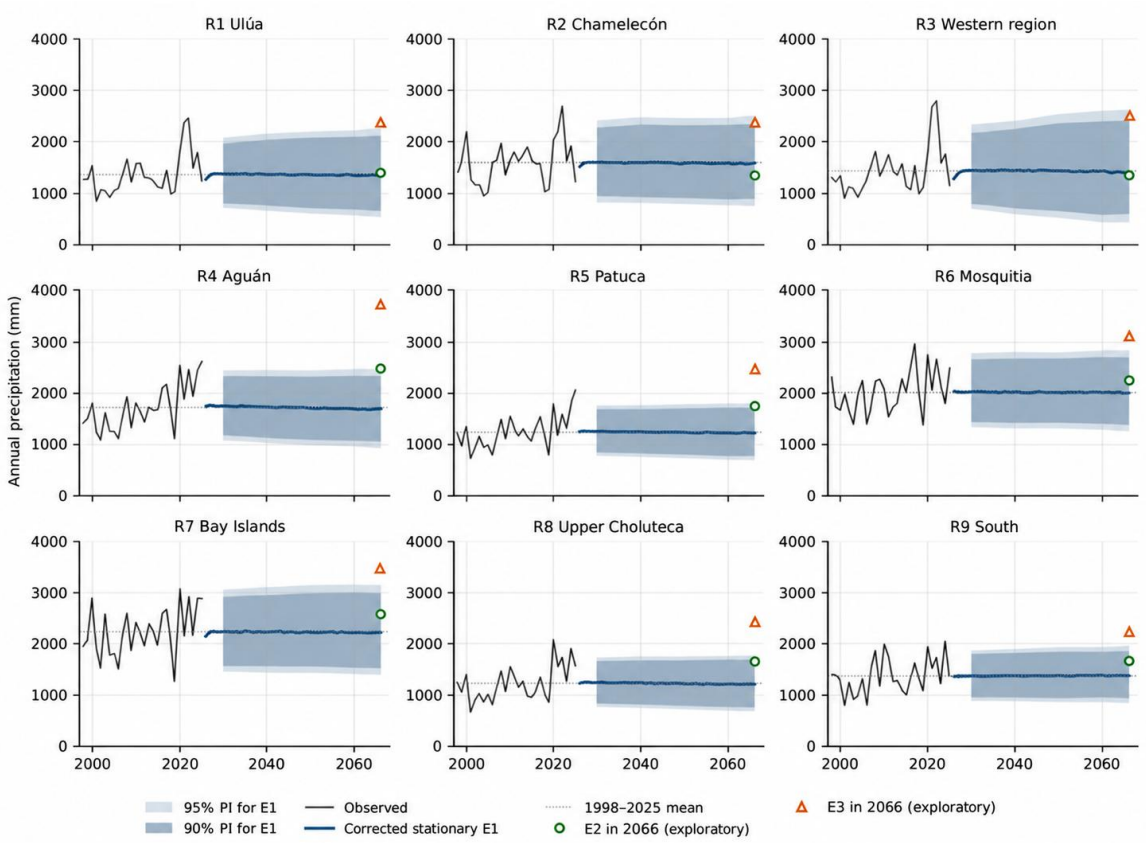

Note: Authors' elaboration with data from NASA POWER (16). The bands are plotted from 2030 by linearly interpolating the percentiles of table S7. E2 and E3 are shown only in 2066 due to their exploratory nature.

DISCUSSION

4.1 Scope of claims

The results support three statements with different degrees of support. The first, descriptive, is that the geography of rainfall remains stable: the gradient between the Caribbean coast and the Pacific slope persists in all the years of the record. The second, also descriptive, is that interannual variability, with coefficients of variation of 20 to 31 percent, is the dominant characteristic of the regime. The third, conditioned by the data product, is that the NASA POWER series shows an increase in rainfall between 1998 and 2025, significant in five of the nine regions even correcting for autocorrelation, which depends on the wet block from 2020 to 2025 and disappears when it is excluded.

The results do not support that rainfall in Honduras has increased in a climatic sense or that it will continue to increase. The analysis rests on a single reanalysis product, without contrast with rainfall stations or with another independent product, and the reanalysis itself may present drifts; that is why the trends are presented as properties of the NASA POWER series and not as observed and confirmed changes in the country. A twenty-eight-year window also does not separate a wet phase trend from a low-frequency oscillation, and physics-based climate projections point in the opposite direction. Finally, the models evaluated did not allow the total of a specific year to be forecasted: in the

validation they left errors in the order of 25 percent and none convincingly exceeded the repetition of the historical average.

This negative result retains practical utility within its scope. For the models and validation period studied, an error of 25 percent over a total of 1,500 millimeters is equivalent to about 375 millimeters, on the order of the distance between a good and a bad year. The annual distribution, moreover, is asymmetrical to the right in eight of the nine regions, and in those same eight at least 15 of the 28 years of the record are below the average, so that the mean misdescribes the typical year. Whether or not this property translates into failures of a reservoir or irrigation system depends on flows, storage, and demand that this paper does not analyze. What the study provides is a description of the distribution of annual rainfall and its uncertainty, with the caveat that the prediction intervals underestimated the frequency of wet years in the validation.

4.2 The discrepancy with climate models

The CMIP6 set systematized by the World Bank projects for Honduras, compared to its reference period of 1995 to 2014, a reduction of 53 millimeters per year for 2040-2059 and 71 millimeters for 2080-2099 under the SSP2-4.5 scenario. Under SSP5-8.5 the reduction is 140 and 365 millimeters, in the latter case about 22 percent of the reference rainfall (25). These figures coincide in the direction of the First Communication on Adaptation and the National Plan for Drinking Water and Sanitation (5,6).

The portal itself indicates that these anomalies must be interpreted with respect to their historical reference period (25), which does not coincide with that of this study, and the horizons are not the same either. To make the magnitudes comparable, Figure 6 shows all the figures as anomalies: those of this study with respect to the national average from 1998 to 2014 (1 357 millimetres), the sub-period of the record closest to 1995-2014, and those of CMIP6 with respect to 1995-2014. With this common basis, the observed series from 2015 to 2025 is 328 millimetres above the reference, corrected E1 is 126 millimetres above in 2040-2059, and CMIP6 projects reductions of 53 to 140 millimetres for the same period.

Figure 6.

Anomalies of annual precipitation in this study and CMIP6 projections for their reference periods

https://doi.org/10.71068/SDIJ0108

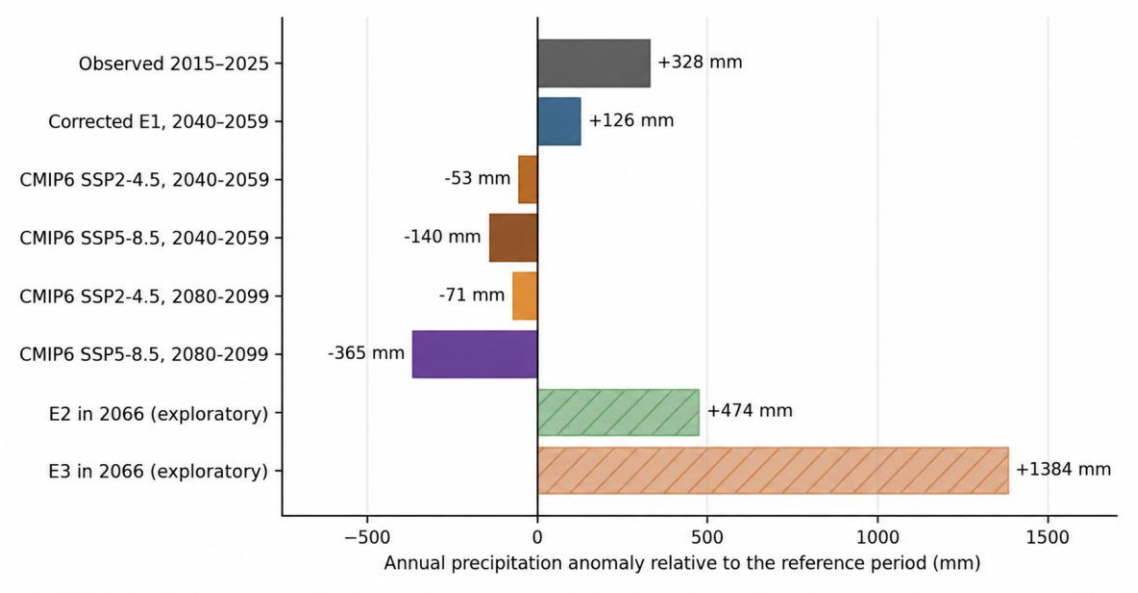

Note: Prepared by the authors with data from NASA POWER (16) and the World Bank (25). Reference: national area-weighted average from 1998 to 2014 for this study and 1995 to 2014 for CMIP6. E2 and E3 are plotted due to their exploratory nature and correspond to another horizon (2066).

The discrepancy does not imply an error on either side. The statistical models extrapolate what happened between 1998 and 2025, a period in which the series of reanalyses shows an increase in rainfall in Honduras; climate models simulate the physical response of the atmosphere to radiative forcing, which in Central America points to drying. Three explanations are compatible with the data and are not mutually exclusive. The first is that the period analyzed coincides with a wet phase of the Atlantic multidecadal variability, so that the trend is real but transient. The second is that the MERRA-2 reanalysis shows a drift of its own in the region, a possibility that can only be ruled out by comparing it with station records. The third is that global climate models misrepresent precipitation in Central America, a region with complex topography and small scale compared to its resolution, where the sign of the projected change is less consistent than that of temperature.

Even with a common basis, the two families of figures are not equivalent estimates of the same magnitude: one extrapolates the statistics of a period, the other simulates the response to a force, and differ in horizon. That is why this work does not combine their values in a single range for 2066. The useful reading is more modest: the sign of future rainfall change in Honduras is uncertain, and the distance between corrected E1 and the CMIP6 projections, from 180 to 490 millimeters depending on the scenario and the horizon, is of the same order as the interannual variability that the country is already experiencing.

4.3 Variability as a dominant trait

Below the discrepancy on the mean level, the record shows a rapid alternation between extreme years: four of the five wettest years of the three decades occurred from 2020 onwards and the driest was 2019, immediately before. This work did not analyse the frequency or intensity of extreme events, which require daily or sub-daily data, so that this alternation does not allow us to say that extremes are becoming more frequent. It does allow us to affirm that the succession of very different

years is a feature of the recent period, and is the one that is least tolerated by a rainfed agricultural system or a system of reservoirs without multi-year regulation capacity.

The 2026 season offers a real-time demonstration. An exceptionally rainy April, followed by a May-August season with deficits of between 25 and 48 percent in five of the nine regions, produced a near-normal cumulative and severe supply crisis in the capital. The annual average said nothing useful about what was happening.

4.4 Sectoral implications

4.4.1 Crops

Corn, beans, and sorghum are produced in rainfed areas and in two cycles separated by the heat wave, which makes them sensitive to the distribution of rainfall within the season much more than to their annual total. The Honduran dry corridor covers 146 municipalities in 13 departments, and the 2015 El Niño episode affected 161,403 producing families (1). In 2022, 512,413 quintals of beans, corn, and sorghum were lost in the first cycle alone (5), on an adjusted national balance: bean production in 2025 was between 3.5 and 3.8 million quintals against a demand of close to 3.6 million (26).

The results allow us to specify where the risk is at play. In the corrected stationary scenario, the southern region projects a median of 1 366 millimeters for 2066 with a 90 percent prediction interval of 926 to 1 832. Values below this lower limit already occurred in 2001, with 793 millimeters, and in 2006, with 813. The model does not anticipate a new drought: it indicates that known droughts may recur with similar frequency. For agricultural planning, the lower limit of the distribution is a more informative starting point than the median, although using it for sizing requires specific agronomic and hydrological studies.

Coffee occupies a particular position. In the evaluation of Eta and Iota, it concentrated 49 percent of the damage to the agricultural sector, that is, the destruction of productive capital; in production losses it totaled 272 million lempiras, behind beans with 1,153 million (4). The western region, the main coffee-growing area, is the one with the highest coefficient of variation in the country and the only one where the model left residual autocorrelation uncaptured, so it is both the most difficult to anticipate and the one that concentrates the crop that brings the most foreign exchange: in the 2024-2025 harvest, Honduras exported 5.52 million quintals for 1,964.37 million dollars (27). African palm, bananas and sugarcane, concentrated in the Sula and Aguán valleys, face the opposite problem: the Aguán basin shows the strongest observed trend in the study and is the one that rises the most in the exploratory scenarios E2 and E3, and in a flat area of slow drainage more rain means more days with saturated soil.

4.4.2 Drinking water supply

Honduras reached 95.69 percent water coverage from improved sources in 2020, but safe water management reaches only 25.10 percent of the population, the average continuity of urban service is 13 hours per day, and non-revenue water in the main urban providers amounts to 47.76 percent

(6). These figures change the way projections are read: a 10 percent reduction in precipitation, which is approximately what the moderate climate scenario projects, is equivalent to less than a quarter of what is currently lost in the networks.

Tegucigalpa concentrates the problem in its most acute form. The capital is supplied by the Los Laureles and La Concepción reservoirs, both in the upper basin of the Choluteca River, which is the region with the least rainfall of the nine. As of August 14, 2026, they were operating at 38 and 30 percent of their capacity, with rationing that had gone from seven to nine days between June and August; below 20 percent capacity, sediments complicate treatment and below 15 percent the water is no longer usable (28). The data from this study place the episode: the region accumulated 392 millimeters between May and August against an average of 605, with July 40 percent below normal, while the accumulated from January to August ended 29 percent above the average due to the effect of April. A reservoir does not take advantage of an April rain in the same way as a July rain: the former falls on dry soil that absorbs it, the latter drains into the glass.

None of the projections in this work anticipate a new structural shortage for that basin. The median of 2066 in the corrected stationary scenario is 1 200 millimeters, practically equal to the historical average of 1 222, and the lower limit of the 90 percent prediction interval is 763 millimeters, a value that the region already exceeded downwards in 2001, with 661. A system sized for the average can fail in those years; how much depends on storage capacity, losses and demand, variables that this study does not model. The answer options include storage, loss reduction and protection of the basins that feed the reservoirs.

4.4.3 Hydropower generation and irrigation

The sensitivity of the electricity system was documented in 2015, when drought reduced the available generation at the El Cajón plant (5), which is fed by the upper Ulúa basin, by about 40 megawatts. The corrected stationary projection for that basin in 2066 is 1,365 millimeters with a 90 percent prediction interval from 646 to 2,117. In a multi-year regulation reservoir, what is decisive is the succession of dry years and not an isolated year, and the record contains an episode of six consecutive years below the average between 2001 and 2006, with 838, 1,068, 1,047, 926, 1,054 and 1,096 millimeters. An equivalent episode in the 2050s would foreseeably find a higher demand; its effect on generation requires a hydrological and operation analysis of the reservoir that exceeds this work.

Irrigation consumes more than half of the water withdrawn and operates on some 90,000 hectares against a national target of 400,000 hectares (1). Expanding the area under irrigation is the conventional response to variability, and on the Pacific slope it finds a clear limit: the water that would be used for irrigation comes from the same basins that fail in dry years, so expanding irrigation without expanding storage transfers the problem downstream.

4.5 Limitations

Several limitations limit the reading of the results. The first is the dependence on a single reanalysis product without independent validation: the trends and levels are those of NASA POWER and could differ from those of the rainfall stations or other products. The second is spatial representativeness:

the resolution of about 55 by 67 kilometers smooths the orographic maxima, and the values obtained for the Atlantic coast are below the range of 3 000 to 3 300 millimeters that the First Adaptation Communication reports for Atlántida and La Mosquitia (5); in addition, the sampled cells cover 49 percent of the territory, and in R2, R3 and R8 one cell is repeated.

The third is the length of the record, twenty-eight full years, which is sufficient to estimate an average and seasonality but not to separate a genuine trend from a multidecadal oscillation. The fourth is that the models do not incorporate oceanic covariates or external forcings, and their prediction intervals only propagate the variability of innovations, which partly explains their undercoverage in the validation. And any statistical extrapolation assumes that the structure that generates the data will remain in force, an assumption that climate change calls into question.

These constraints define the priority lines for future work: to contrast the series with the national rainfall network and with stand-alone products, to replace three-point sampling with full area-weighted spatial averages, to evaluate non-negative specifications on a monthly scale, and to analyse the frequency and intensity of extremes with daily data.

CONCLUSIONS

The descriptive results, verified within the data product used, are three. The average rainfall in Honduras between 1998 and 2025 was 1,486 millimeters per year weighted by area and 1,572 as a simple average of nine hydrographic regions, with regional averages of 1,222 in the upper Choluteca River basin to 2,229 in the Bay Islands and coefficients of variation of 20 to 31 percent. The annual cycle is bimodal on the Pacific slope, with a heat wave that reduces rainfall in July by between 26 and 44 percent compared to June, and unimodal with a maximum in October and November on the Caribbean coast. And in 2026, an exceptionally rainy April masked a deficit from May to August of up to 48 percent on the Pacific slope, so that the annual accumulated is an insufficient indicator to follow the season.

Statistical trends are conditional on the data product. The NASA POWER series shows positive slopes in all nine regions, from 13.7 to 37.5 millimeters per year, significant in five even correcting for autocorrelation, but none are significant when excluding the wet period from 2020 to 2025. As long as they are not contrasted with seasonal records, they should not be interpreted as an observed climate change in Honduras.

The prospective scenarios are exploratory in nature. No model substantially outperformed climatology in validation, integrated models are inadequate at forty-year because their forecast variance grows without limit, and approximate stationary distributions covered less than half of the validation years; this does not constitute direct evidence of coverage of the model intervals. Corrected for truncation bias, the stationary scenario reproduces climatology, with a national median of 1 468 millimeters in 2066; the dampened and sustained trend scenarios, of 1 831 and 2 742 millimeters, describe assumptions and not forecasts. The CMIP6 projections, of the opposite sign, refer to another reference period and other horizons, so they are not combined with those of this work in a single range.

https://doi.org/10.71068/SDIJ0108

BIBLIOGRAPHIC REFERENCES

1. La Prensa. Tegucigalpa could face water rationing of up to 11 days. La Prensa. August 14, 2026. https://www.laprensa.hn/honduras/tegucigalpa-racionamiento-agua-11-dias-sequia-CE31717432
2. Global Water Partnership Central America. Situation of water resources in Honduras. GWP Central America; 2016. https://www.gwp.org/globalassets/global/gwp-cam_files/srh_honduras_2016.pdf
3. Ministry of Energy of Honduras. Annual statistical report of the national electricity sector 2024. National Electric System; 2025. https://sen.hn/wp-content/uploads/2025/08/IEASEN-2024.pdf
4. Food and Agriculture Organization of the United Nations. The hydrometeorological threat in Honduras in the context of climate change. FAO; 2009. https://www.fao.org/4/i1255b/i1255b01.pdf
5. Economic Commission for Latin America and the Caribbean, Inter-American Development Bank. Assessment of the effects and impacts of tropical storm Eta and Hurricane Iota in Honduras. Inter-American Development Bank; 2021. https://publications.iadb.org/publications/spanish/document/Evaluacion-de-los-efectos-e-impactos-de-la-tormenta-tropical-Eta-y-el-huracan-Iota-en-Honduras..pdf
6. Government of Honduras. First Communication on Adaptation of Honduras. United Nations Framework Convention on Climate Change; 2025. https://unfccc.int/sites/default/files/2025-05/Primera%20Comunicaci%C3%B3n%20de%20Adaptaci%C3%B3n%2C%20Honduras.pdf
7. National Autonomous Aqueduct and Sewerage Service. National Plan for Drinking Water and Sanitation 2022-2030. SANAA; 2022. https://sanaa.hn/wp-content/uploads/2025/06/1.-PLANASA-2022-2030-Version-ampliada.pdf
8. González-Méndez I, Pons D, Anderson TG, Ayes Rivera I, Anchukaitis KJ. Impacts of spatial and temporal station availability on gridded precipitation products in Central America. Earth Space Sci. 2025; 12(12):e2025EA004720. https://doi.org/10.1029/2025EA004720.
9. Alfaro-Córdoba M, Mora-Sandí NP, Hidalgo HG, Alfaro EJ. Central American climate extreme trends: a statistical analysis of CLIMDEX indices. Int J Climatol. 2024; 44(11):4115-26. https://doi.org/10.1002/joc.8571.
10. Kowal KM, Slater LJ, García López A, Van Loon AF. A comparison of seasonal rainfall forecasts over Central America using dynamic and hybrid approaches from Copernicus Climate Change Service seasonal forecasting system and the North American Multimodel Ensemble. Int J Climatol. 2023; 43(5):2175-99. https://doi.org/10.1002/joc.7969.
11. Andrade-Gómez L, Cavazos T. Historical meteorological droughts over the CORDEX-CAM (Central America, Caribbean and Mexico) domain: evaluating the simulation of dry hot spots with RegCM4. Int J Climatol. 2024; 44(4):1110-34. https://doi.org/10.1002/joc.8374.
12. García-Franco JL, Jaramillo A, Dominguez C, Tippett MK, Muñoz ÁG. Subseasonal prediction of the rainy season and the midsummer drought in Mesoamerica. J Geophys Res Atmos. 2025; 130(20):e2025JD044023. https://doi.org/10.1029/2025JD044023.
13. Peña Salinas EJ. Impact of unsustainable forestry practices on carbon sequestration: evidence from tropical ecosystems in Honduras. Imperium Académico Multidiscip J. 2026; 3(1):1-12. https://doi.org/10.63969/mvfgy405.

14. Rodríguez Saldaña NM, Rodriguez Estrella DA. Public Health and Climate Change: Epidemiological Impacts and Mitigation Strategies. Educ Regent Multidiscip J. 2025; 2(4):1-13. https://doi.org/10.63969/7swkeh27.
15. Merino Olivo MP. Relationship between climate variability and food resilience of peasant communities in Manabí, Ecuador. J Multidiscip Novel Journeys Explor. 2026; 4(1):1-20. https://doi.org/10.63688/b6mrwx02.
16. Natural Earth. Admin 1 – States, Provinces, 1:10m Cultural Vectors [conjunto de datos]. Natural Earth; [citado 26 oct 2026]. https://www.naturalearthdata.com/downloads/10m-cultural-vectors/
17. NASA Langley Research Center. POWER Monthly and Annual API, versión 2.9.8, parámetro PRECTOTCORR [conjunto de datos]. Prediction of Worldwide Energy Resources; 2026. https://power.larc.nasa.gov/
18. Gelaro R, McCarty W, Suárez MJ, Todling R, Molod A, Takacs L, et al. The Modern-Era Retrospective Analysis for Research and Applications, Version 2 (MERRA-2). J Clim. 2017; 30(14):5419-54. https://doi.org/10.1175/JCLI-D-16-0758.1.
19. Mann HB. Nonparametric tests against trend. Econometrica. 1945; 13(3):245-59. https://doi.org/10.2307/1907187.
20. Kendall MG. Rank correlation methods. 4.ª ed. Londres: Charles Griffin; 1975.
21. Sen PK. Estimates of the regression coefficient based on Kendall's tau. J Am Stat Assoc. 1968; 63(324):1379-89. https://doi.org/10.1080/01621459.1968.10480934.
22. Hamed KH, Rao AR. A modified Mann-Kendall trend test for autocorrelated data. J Hydrol. 1998; 204(1-4):182-96. https://doi.org/10.1016/S0022-1694(97)00125-X.
23. Yue S, Pilon P, Phinney B, Cavadias G. The influence of autocorrelation on the ability to detect trend in hydrological series. Hydrol Process. 2002; 16(9):1807-29. https://doi.org/10.1002/hyp.1095.
24. Hyndman RJ, Athanasopoulos G. Forecasting: principles and practice. 3.ª ed. OTexts; 2021. https://otexts.com/fpp3/
25. Gneiting T, Balabdaoui F, Raftery AE. Probabilistic forecasts, calibration and sharpness. J R Stat Soc Series B Stat Methodol. 2007; 69(2):243-68. https://doi.org/10.1111/j.1467-9868.2007.00587.x.
26. World Bank. Climate Change Knowledge Portal: CMIP6 Projections for Honduras [Dataset]. 2026. https://climateknowledgeportal.worldbank.org/country/honduras
27. Infobae. Unions warn of loss of one million quintals of beans in Honduras. Infobae. May 3, 2026. https://www.infobae.com/honduras/2026/05/03/gremiales-alertan-sobre-perdida-de-un-millon-de-quintales-de-frijol-en-honduras/
28. Forbes Central America. Honduran coffee exports grow by 3% in the 2024-2025 harvest. Forbes Central America. July 15, 2025. https://forbescentroamerica.com/2025/07/15/las-exportaciones-de-cafe-hondureno-crecen-un-3-en-la-cosecha-2024-2025/

ETHICAL CONSIDERATIONS

The study was developed through a literature review based exclusively on previously published documentary sources. It did not involve the direct participation of human or animal beings, the performance of interventions, the use of biological samples, or access to personally identifiable data.

Consequently, it did not require approval from an ethics committee or the obtaining of informed consent. During the research process, the principles of scientific integrity, adequate attribution of authorship, rigorous citation, and responsible use of the sources consulted were observed.

ARTIFICIAL INTELLIGENCE (AI) USAGE STATEMENT

The authors state that the AI tool was used exclusively to support the organization of the article and the translation of the text. Its use did not determine the scientific content, study design, selection of sources, data analysis, interpretation of results, or conclusions. Full responsibility for the content remains with the authors.

FUNDING

The authors state that this study did not receive any external funding from public, private, or non-profit organizations. All research, analysis, and development activities were carried out with their own resources.

CONFLICT OF INTEREST

The authors declare that they have no conflicts of interest related to this study and that all the procedures followed comply with the ethical standards established by the journal. They also confirm that this work is unpublished and has not been published, either partially or totally, in any other publication.

AUTHOR'S CONTRIBUTION

Authors' names and initials: Marco Antonio Ramos Espinal (MARE), Nestor Adrián López Luque (NALL)

1. Conceptualization: MARE, NALL
2. Data curation: MARE, NALL
3. Formal analysis: MARE, NALL
4. Acquisition of financing: not applicable
5. Research: MARE, NALL
6. Methodology: MARE, NALL
7. Project Management: MARE, NALL
8. Remedies: Not applicable
9. Software: Not applicable
10. Supervision: MARE, NALL
11. Validation: MARE, NALL
12. Vista: MARE, NALL
13. Original Draft: MOTHER, NALL
14. Writing, proofreading and editing: MARE, NALLç

SUPPLEMENTARY MATERIAL

This section brings together the tables and supporting figures that are not part of the body of the article. The numbering is prefixed with S to distinguish it from that of the main text.

Table S1.

Sampling points, surface area and coverage of MERRA-2 cells in each region

Region	Point 1	Point 2	Point 3	Area (km²)	Coverage (%)
R1 Ulúa	87.61 W / 14.63 N / 1 015 m	88.06 W / 14.23 N / 927 m	88.36 W / 15.08 N / 718 m	15 928	45
R2 Chamelecón	87.92 W / 15.65 N / 320 m	87.92 W / 15.05 N / 718 m	88.12 W / 15.50 N / 320 m	3 971	86
R3 West	88.56 W / 14.32 N / 1,021 m	89.01 W / 14.52 N / 1,021 m	88.81 W / 14.92 N / 791 m	9 258	66
R4 Aguán	86.39 W / 15.60 N / 540 m	85.39 W / 15.65 N / 471 m	87.39 W / 15.40 N / 406 m	20 593	40
R5 Patuca	86.37 W / 14.96 N / 809 m	86.42 W / 14.11 N / 778 m	85.52 W / 14.81 N / 674 m	31 519	32
R6 Mosquitia	84.60 W / 15.57 N / 21 m	83.85 W / 15.12 N / 27 m	84.55 W / 15.02 N / 81 m	16 043	62
R7 Islands	86.45 W / 16.37 N / 1 m	85.90 W / 16.47 N / 0 m	86.90 W / 16.12 N / 136 m	257	92
R8 Choluteca Alta	87.35 W / 13.91 N / 901 m	87.10 W / 14.36 N / 925 m	87.05 W / 14.71 N / 925 m	8 588	55
R9 On	86.92 W / 13.43 N / 646 m	87.52 W / 13.58 N / 308 m	87.22 W / 13.23 N / 50 m	6 078	86

Note: Coordinates of the points queried in NASA POWER and average elevation that the system assigns to the cell that contains them. In R2 (points 1 and 3), R3 (points 1 and 2) and R8 (points 2 and 3) two points fall in the same cell of MERRA-2, which therefore weighs twice as much in the regional average. The area was calculated with the limits of Natural Earth (7) in cylindrical projection of equal areas; the coverage is the proportion of that area located within the sampled cells. The cells represented do not cover the entire regional area and the original series per cell do not appear in the table; the remaining figures retain the values of the initial sampling.

Table S2.

Selected models by region and waste diagnosis

Region	SARMA Model	AICc	σ (mm)	Ljung-Box denomination p	a	f
R1 Ulúa	$(2,0,2)\ (2,0,1)_{12}$	3 713	57,4	0,067	0,150	0,804
R2 Chamelecón	$(1,0,1)\ (1,0,1)_{12}$	3 816	68,0	0,611	0,159	0,800
R3 West	$(2,0,2)\ (1,0,1)_{12}$	3 791	65,1	0,029	0,152	0,800
R4 Aguán	$(2,0,0)\ (1,0,1)_{12}$	3 889	76,1	0,873	0,062	0,800
R5 Patuca	$(2,0,0)\ (1,0,1)_{12}$	3 763	63,0	0,862	0,046	0,800
R6 Mosquitia	$(2,0,0)\ (1,0,1)_{12}$	4 093	102,3	0,453	0,014	0,935
R7 Bay Islands	$(2,0,1)\ (1,0,2)_{12}$	4 095	101,9	0,532	0,018	0,800
R8 Choluteca Alta	$(1,0,0)\ (1,0,1)_{12}$	3 743	61,1	0,948	0,065	0,973
R9 On	$(2,0,0)\ (1,0,1)_{12}$	3 856	70,7	0,738	0,044	0,957

Note: σ is the monthly residual standard deviation of the stationary model. α and ϕ are the level and damping parameters of the Holt-Winters model; β and γ were estimated at zero in the nine regions. Authors.

https://doi.org/10.71068/SDIJ0108

Table S3.

Precipitation from May to August 2026 vs. the average 1998 to 2025

Region	May-ago 2026 (mm)	Average (mm)	Abnormality (%)	July 2026 anomaly (%)
R1 Ulúa	421	665	−37	−63
R2 Chamelecón	482	641	−25	−71
R3 West	452	705	−36	−68
R4 Aguán	553	568	−3	+24
R5 Patuca	508	552	−8	+32
R6 Mosquitia	832	828	0	+44
R7 Bay Islands	576	728	−21	+36
R8 Choluteca Alta	392	605	−35	−40
R9 On	373	717	−48	−70

Note: Rebuilt from the NASA POWER Daily Interface (8).

Table S4.

Honduras Power Generation by Source, 2024

Source	Generation (GWh)	Participation (%)	Installed capacity (MW)
Thermal with bunker and diesel	5 028,71	40,50	1 210,6
Hydroelectric	3 834,13	30,88	927,4
Solar	1 020,04	8,21	549,9
Petroleum coke	871,85	7,02	105,0
Biomass	691,71	5,57	239,8
Wind	665,73	5,36	238,1
Geothermal	304,84	2,46	40,0
Total	12 416,80	100,00	3 310,83

Note: Source: Ministry of Energy (2).

Table S5.

Annual Observed Precipitation by Region, 1998 to 2025

Year	R1	R2	R3	R4	R5	R6	R7	R8	R9	Simple	Weighted
1998	1274	1399	1307	1397	1173	2261	1945	1240	1390	1487	1422
1999	1270	1692	1226	1501	939	1730	2042	1046	1400	1427	1288
2000	1535	2195	1342	1802	1354	1673	2852	1387	1278	1713	1538
2001	838	1261	901	1226	750	1972	1875	661	793	1142	1053
2002	1068	1155	1127	1089	926	1632	1537	916	1247	1188	1120
2003	1047	1170	1078	1618	1157	1404	2548	1045	918	1332	1237
2004	926	944	915	1253	946	1956	1769	861	1002	1175	1140
2005	1054	1016	1087	1260	975	2211	1813	1024	1303	1305	1249
2006	1096	1610	1273	1129	786	1416	1507	817	813	1161	1058
2007	1354	1634	1503	1571	1141	1746	2218	1144	1510	1536	1407
2008	1650	1957	1797	1902	1464	2206	2570	1440	1830	1868	1742
2009	1219	1363	1326	1337	1096	2240	1866	1062	1155	1407	1352
2010	1561	1629	1500	1773	1504	2059	2400	1527	1969	1769	1674
2011	1572	1787	1736	1648	1284	1536	2265	1352	1742	1658	1515
2012	1300	1612	1431	1442	1154	1726	1970	1138	1264	1449	1355

https://doi.org/10.71068/SDIJ0108

Year	R1	R2	R3	R4	R5	R6	R7	R8	R9	Simple	Weighted
2013	1302	1728	1342	1714	1295	1793	2392	1267	1273	1568	1462
2014	1234	1888	1561	1672	1152	2255	2246	975	1126	1568	1464
2015	1127	1632	1146	1670	1068	2007	1974	961	994	1398	1337
2016	1096	1570	1073	2074	1332	2467	2578	1088	1316	1621	1567
2017	1432	1583	1522	2137	1503	2948	2648	1346	1595	1857	1816
2018	982	1027	986	1689	1214	1895	2100	1050	1303	1361	1334
2019	1042	1067	1123	1116	778	1383	1255	853	1102	1080	1027
2020	1816	2030	1763	2525	1749	2734	3049	2065	1904	2182	2088
2021	2365	2177	2667	1878	1175	2055	2146	1538	1519	1947	1806
2022	2451	2676	2788	2419	1555	2656	2917	1712	1731	2323	2164
2023	1463	1623	1578	1928	1291	2090	2149	1261	1215	1622	1577
2024	1790	1910	1743	2403	1712	1808	2892	1884	2032	2019	1906
2025	1243	1233	1151	2597	2041	2481	2882	1553	1376	1840	1919

Note: Values in millimeters per year. Simple is the simple average of the nine regions and weighted the weighted average by area. Prepared by the authors with data from NASA POWER (8).

Table S6.

Projected annual precipitation in the corrected stationary scenario, 2026 to 2066

Year	R1	R2	R3	R4	R5	R6	R7	R8	R9	Simple	Weighted
2026	1270	1520	1283	1746	1255	2027	2154	1227	1348	1537	1474
2027	1356	1602	1396	1766	1263	2014	2234	1243	1354	1581	1504
2028	1375	1601	1428	1747	1254	2015	2239	1248	1362	1585	1505
2029	1373	1616	1442	1744	1254	2015	2231	1236	1351	1585	1504
2030	1368	1602	1438	1752	1258	2024	2239	1236	1367	1587	1507
2031	1369	1610	1438	1743	1254	2021	2239	1250	1360	1587	1505
2032	1365	1604	1437	1735	1247	2025	2227	1233	1357	1581	1500
2033	1375	1607	1431	1729	1251	2018	2235	1230	1358	1582	1500
2034	1372	1599	1441	1745	1247	2012	2222	1234	1358	1581	1501
2035	1375	1600	1434	1733	1248	2012	2249	1234	1360	1583	1499
2036	1360	1581	1438	1735	1245	2013	2240	1239	1359	1579	1497
2037	1367	1596	1449	1728	1245	2006	2223	1233	1362	1579	1497
2038	1375	1600	1447	1721	1239	2019	2237	1236	1361	1582	1497
2039	1366	1596	1437	1719	1246	2012	2230	1235	1369	1579	1496
2040	1362	1598	1439	1719	1243	2020	2235	1238	1359	1579	1495
2041	1364	1597	1446	1715	1236	2014	2240	1224	1364	1578	1492
2042	1364	1602	1432	1709	1234	2001	2240	1233	1360	1575	1488
2043	1371	1601	1447	1717	1235	2004	2249	1219	1360	1578	1491
2044	1364	1604	1429	1717	1230	2005	2221	1227	1362	1573	1488
2045	1353	1600	1441	1710	1235	2018	2234	1226	1362	1575	1489
2046	1357	1602	1449	1710	1233	2022	2230	1219	1358	1576	1490
2047	1360	1593	1442	1706	1231	2008	2214	1225	1358	1571	1486
2048	1364	1581	1433	1709	1235	2009	2224	1226	1360	1571	1488
2049	1363	1569	1433	1696	1229	2010	2236	1221	1360	1569	1483
2050	1362	1588	1432	1692	1230	2008	2223	1211	1364	1568	1482
2051	1356	1586	1429	1684	1224	2004	2224	1210	1359	1564	1477
2052	1357	1596	1431	1685	1219	2010	2221	1216	1347	1565	1477
2053	1357	1588	1416	1698	1219	2012	2227	1213	1354	1565	1478
2054	1357	1588	1419	1685	1222	2010	2228	1202	1362	1564	1476
2055	1356	1580	1426	1683	1236	2015	2237	1214	1363	1568	1482
2056	1348	1577	1413	1680	1223	2004	2213	1210	1366	1559	1473

Year	R1	R2	R3	R4	R5	R6	R7	R8	R9	Simple	Weighted
2057	1352	1579	1420	1685	1224	2013	2235	1203	1365	1564	1477
2058	1365	1585	1428	1684	1218	2013	2220	1203	1363	1564	1477
2059	1362	1579	1418	1681	1214	2017	2219	1207	1370	1563	1475
2060	1342	1590	1429	1671	1214	2006	2219	1207	1370	1561	1470
2061	1349	1573	1417	1666	1212	2015	2225	1210	1353	1558	1469
2062	1344	1579	1390	1674	1207	2010	2213	1205	1362	1554	1466
2063	1349	1588	1408	1661	1216	2007	2218	1206	1357	1557	1468
2064	1357	1568	1405	1663	1223	2021	2214	1204	1364	1558	1472
2065	1346	1582	1393	1675	1212	1994	2222	1211	1363	1555	1466
2066	1365	1584	1410	1671	1204	2006	2223	1200	1366	1559	1468

Note: Median of 5 000 simulated trajectories multiplied by the truncation bias correction factor for each region (Table S10), in millimeters per year. Simple and weighted as in Table S5. Prepared by the authors with data from NASA POWER (8).

Table S7.

Corrected Stationary Scenario Prediction Intervals in Selected Years

Region	Year	Medium (mm)	IP 90 %	IP 95 %
R1 Ulúa	2030	1368	809 a 1962	730 a 2074
R1 Ulúa	2040	1361	765 a 2036	667 a 2161
R1 Ulúa	2050	1361	710 a 2071	603 a 2193
R1 Ulúa	2060	1342	684 a 2086	566 a 2219
R1 Ulúa	2066	1364	646 a 2116	542 a 2274
R2 Chamelecón	2030	1602	951 a 2278	819 a 2414
R2 Chamelecón	2040	1598	919 a 2330	810 a 2473
R2 Chamelecón	2050	1588	901 a 2314	785 a 2459
R2 Chamelecón	2060	1590	875 a 2325	758 a 2455
R2 Chamelecón	2066	1584	886 a 2341	751 a 2513
R3 West	2030	1439	802 a 2175	711 a 2333
R3 West	2040	1440	701 a 2257	582 a 2399
R3 West	2050	1433	649 a 2356	516 a 2532
R3 West	2060	1430	573 a 2389	442 a 2602
R3 West	2066	1411	586 a 2407	443 a 2615
R4 Aguán	2030	1753	1189 a 2330	1093 a 2434
R4 Aguán	2040	1720	1125 a 2320	1032 a 2442
R4 Aguán	2050	1692	1082 a 2306	984 a 2431
R4 Aguán	2060	1672	1063 a 2322	967 a 2466
R4 Aguán	2066	1672	1053 a 2311	929 a 2451
R5 Patuca	2030	1258	856 a 1667	780 a 1746
R5 Patuca	2040	1243	821 a 1669	758 a 1749
R5 Patuca	2050	1229	797 a 1677	719 a 1767
R5 Patuca	2060	1213	762 a 1693	685 a 1782
R5 Patuca	2066	1203	770 a 1693	683 a 1789
R6 Mosquitia	2030	2025	1436 a 2654	1332 a 2770
R6 Mosquitia	2040	2021	1408 a 2665	1305 a 2799
R6 Mosquitia	2050	2009	1411 a 2663	1304 a 2780
R6 Mosquitia	2060	2007	1392 a 2688	1275 a 2820
R6 Mosquitia	2066	2007	1369 a 2681	1248 a 2821

https://doi.org/10.71068/SDIJ0108

Region	Year	Medium (mm)	IP 90 %	IP 95 %
R7 Islands	2030	2239	1580 a 2927	1472 a 3058
R7 Islands	2040	2235	1563 a 2945	1425 a 3086
R7 Islands	2050	2224	1557 a 2970	1427 a 3119
R7 Islands	2060	2219	1527 a 2978	1402 a 3118
R7 Islands	2066	2224	1521 a 2959	1393 a 3089
R8 Choluteca Alta	2030	1236	845 a 1657	774 a 1725
R8 Choluteca Alta	2040	1239	820 a 1669	743 a 1755
R8 Choluteca Alta	2050	1212	795 a 1670	720 a 1756
R8 Choluteca Alta	2060	1208	771 a 1676	693 a 1755
R8 Choluteca Alta	2066	1201	763 a 1681	683 a 1772
R9 On	2030	1367	957 a 1789	884 a 1874
R9 On	2040	1359	956 a 1807	885 a 1877
R9 On	2050	1364	940 a 1826	868 a 1919
R9 On	2060	1370	947 a 1820	859 a 1902
R9 On	2066	1366	926 a 1832	849 a 1931

Note: The intervals are for prediction for the annual total of the year indicated and not for the average of the period. Values multiplied by the correction factor in table S10. Prepared by the authors with data from NASA POWER (8).

Table S8.

Average annual cycle of precipitation by region, in millimeters per month

My	R1	R2	R3	R4	R5	R6	R7	R8	R9
January	43	106	48	141	54	100	186	31	6
February	30	69	34	81	35	68	102	20	6
March	46	77	56	80	52	52	78	31	13
April	40	43	39	44	35	59	51	40	37
May	150	128	147	98	109	141	108	140	190
June	205	187	213	163	169	221	200	194	229
July	145	164	158	163	144	265	221	132	128
August	166	162	187	145	130	201	198	139	170
September	208	183	213	154	148	168	196	189	271
October	175	192	169	235	171	313	337	173	237
November	87	158	91	234	109	261	330	75	55
December	68	121	74	169	76	162	221	58	19

Note: The region codes correspond to those in Table 1. Prepared by the authors with data from NASA POWER (8).

Table S9.

Mann-Kendall Statistics and Stationarity Tests by Region, 1998 to 2025

Region	Mann-Kendall Z	ADF p-value	KPSS p-value
R1 Ulúa	1,96	0,028	0,015
R2 Chamelecón	1,28	0,025	0,096
R3 West	2,27	0,021	0,014
R4 Aguán	3,81	0,016	0,010
R5 Patuca	3,06	0,020	0,010
R6 Mosquitia	1,92	0,003	0,100
R7 Bay Islands	2,27	0,000	0,100
R8 Choluteca Alta	2,43	0,003	0,016
R9 On	1,62	0,001	0,100

Note: ADF is the augmented Dickey-Fuller test, whose null hypothesis is the unit root; KPSS inverts the null hypothesis. Both were applied to the monthly series. A p-value of 0.100 in KPSS indicates that the statistic was left out of the table of critical values on the non-significance side. Authors' elaboration with data from NASA POWER (8).

Table S10.

Truncation bias of the stationary scenario and contrast with a non-negative gamma distribution

Region	Observed Mean (mm)	Level E1 uncorrected (mm)	Bias (mm)	Bias (%)	Factor	Mid Range (mm)	Gamma IP 90 %	Gamma IP 95 %
R1 Ulúa	1 361	1 510	+149	+10,9	0,901	1 331	836 a 1 989	759 a 2 136
R2 Chamelecón	1 592	1 648	+56	+3,5	0,966	1 558	995 a 2 303	906 a 2 468
R3 West	1 428	1 560	+132	+9,2	0,916	1 391	842 a 2 141	757 a 2 309
R4 Aguán	1 706	1 907	+201	+11,8	0,895	1 672	1 084 a 2 443	991 a 2 613
R5 Patuca	1 233	1 378	+146	+11,8	0,894	1 209	788 a 1 758	721 a 1 879
R6 Mosquitia	2 012	2 137	+125	+6,2	0,942	1 986	1 409 a 2 704	1 313 a 2 858
R7 Bay Islands	2 229	2 374	+145	+6,5	0,939	2 196	1 518 a 3 051	1 407 a 3 236
R8 Choluteca Alta	1 222	1 405	+183	+15,0	0,870	1 195	751 a 1 786	681 a 1 918
R9 On	1 361	1 517	+156	+11,5	0,897	1 334	867 a 1 945	793 a 2 080
National, weighted	**1 486**	**1 639**	**+152**	**+10,2**	**0,907**			

Note: The uncorrected level is the average of the E1 medians between 2027 and 2066; the factor is the quotient between the observed mean and that level, and multiplies the E1 medians and percentiles in tables 4, S6, and S7. The gamma distribution was adjusted for maximum likelihood to the annual totals from 1998 to 2025, and its intervals are predictive for any given year under stationarity. Prepared by the authors with data from NASA POWER (8).

https://doi.org/10.71068/SDIJ0108

Figure S1.

Annual anomaly of average rainfall for the nine regions compared to the average 1998 to 2025

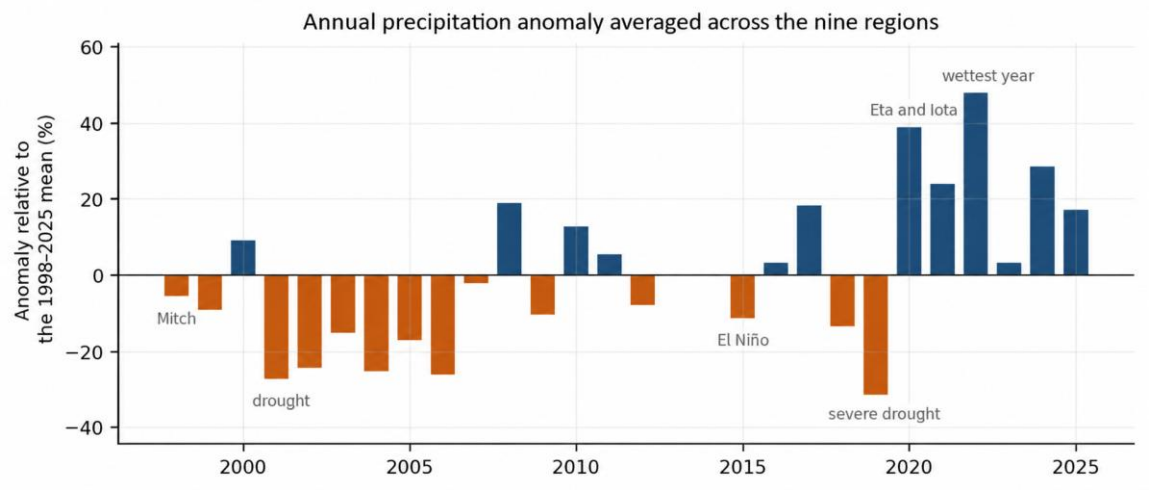

Note: Own elaboration with data from NASA POWER (8).

Figure S2.

Average model error over annual totals in the validation window, 2019 to 2025

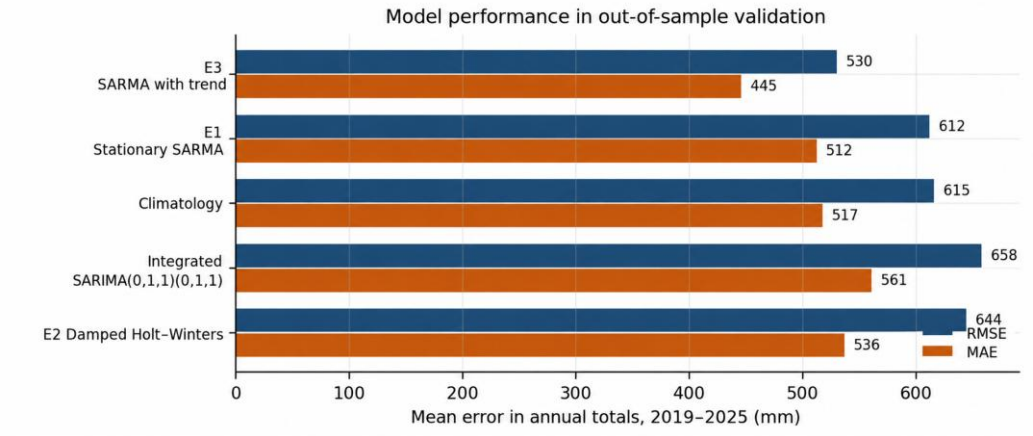

Note: Own elaboration with data from NASA POWER (8).

https://doi.org/10.71068/SDIJ0108

Figure S3.

Growth in the amplitude of the 95 percent range according to the projection horizon, averaged over the nine regions

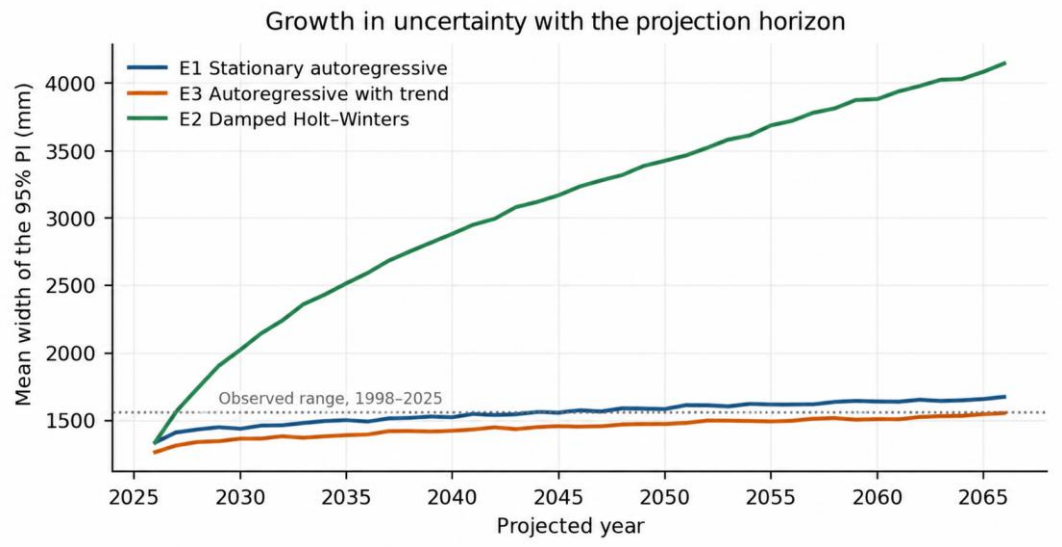

Note: Authors' elaboration with data from NASA POWER (8). Amplitudes of the E1 scenario without correcting for truncation bias; the correction reduces them by 3 to 13 percent.

Figure S4.

Percentage change in annual precipitation to 2066 from the average 1998 to 2025, based on all three scenarios, with E1 corrected

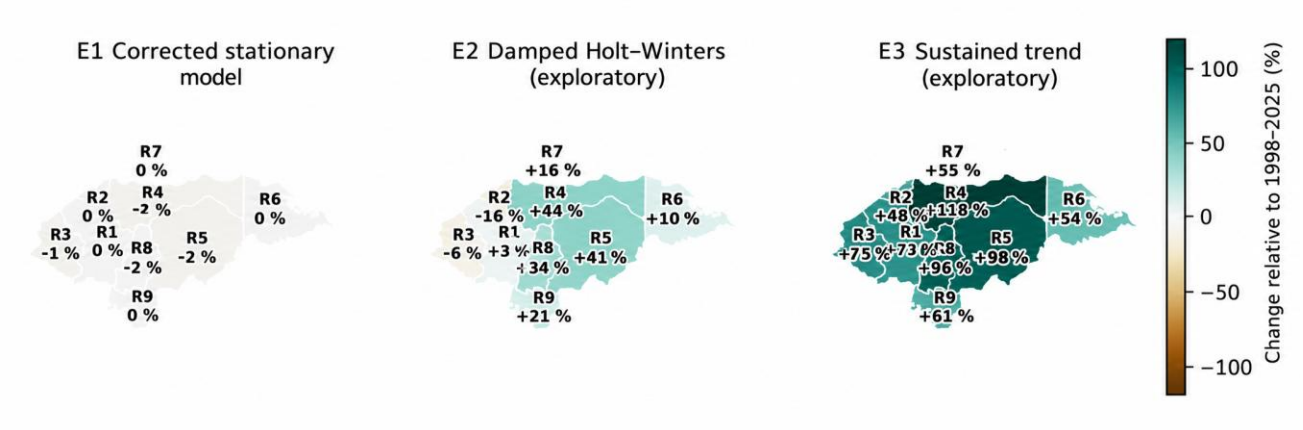

Note: Own elaboration with data from NASA POWER (8).

https://doi.org/10.71068/SDIJ0108

Figure S5.

Chain of transmission between rainfall and water use in Honduras

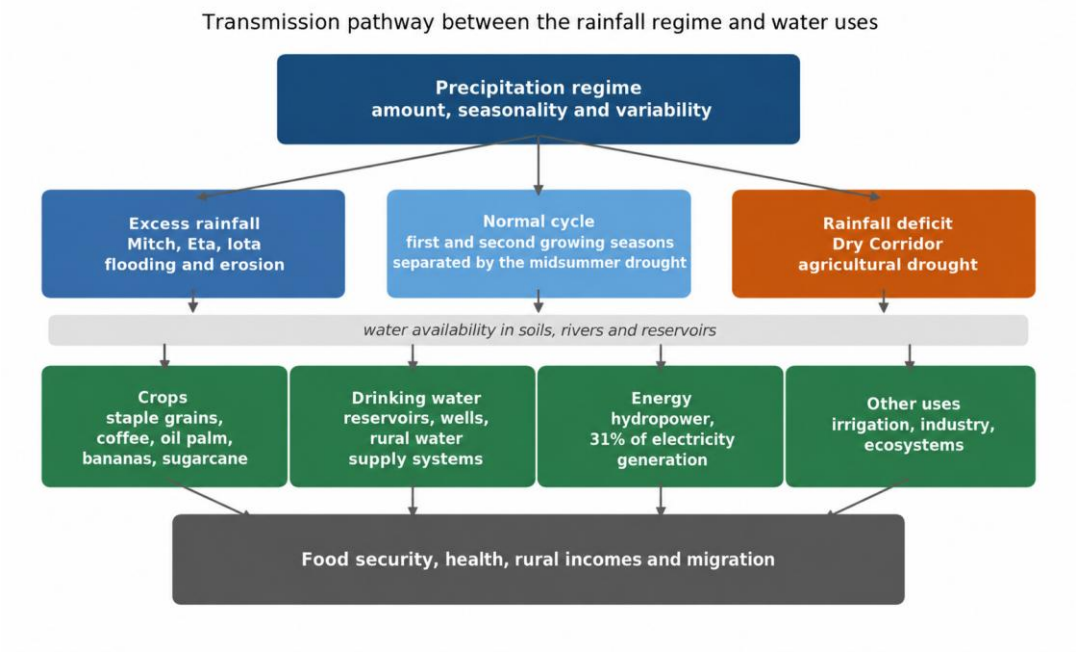

Note: Authors.

Figure S6.

Production losses in the agricultural sector by crop after the passage of Eta and Iota in 2020

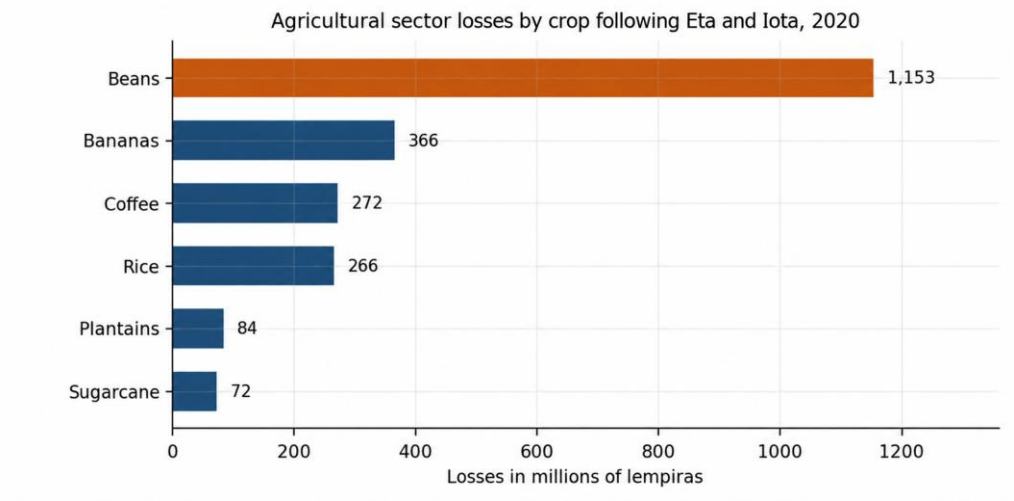

Note: Prepared with data from ECLAC and IDB (4).

https://doi.org/10.71068/SDIJ0108

Figure S7.

Drinking water and sanitation coverage in Honduras

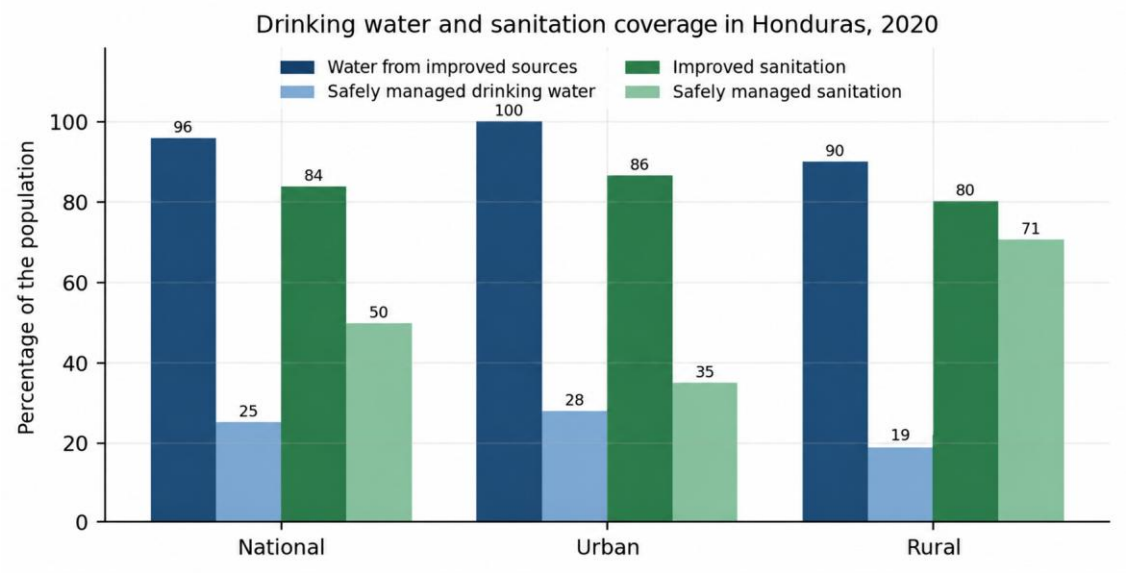

Note: Prepared with SANAA data (6).

https://doi.org/10.71068/SDIJ0108